Journal of Pharmaceutical Innovation (2026) 21:75
https://doi.org/10.1007/s12247-025-10145-x

RESEARCH

# Scouting the Efficacy of Chitosan-coated Litsea Lipid Carriers Nanoplatform as an Oral Delivery System of Lornoxicam in an Inflammatory Animal Model

**Walaa A. El-Dakroury[1] · Abdelrahman R. Said[1] · Gihan F. Asaad[2] · Heba M. I. Abdallah[2] · Marwa E. Shabana[3] · Rahma A. Abdelsalam[4] · Eman M. Elsadek[4] · Basma H. Mohamed[4] · Yara S. Mohamed[4] · Sara M. Seliem[4] · Elsayed Y. Hamada[4] · Belal W. Attef[4] · Sara Saeed Kotb[5] · Shaza H. Aly[5]**

Received: 18 July 2025 / Accepted: 17 September 2025 / Published online: 29 December 2025
© The Author(s) 2025

## Abstract

Lornoxicam-loaded chitosan-coated Litsea lipid nanocarriers (LRX-CS-LLCs) were developed as an innovative oral delivery system, combining the synergistic anti-inflammatory effects of Litsea cubeba oil with the mucoadhesive properties of chitosan. The GC/MS analysis of *Litsea cubeba* oil identified *α*-citral (47.56%), *β*-citral (26.86%), and *D*-limonene (14.00%). Various LRX-loaded LLCs were prepared and optimized. Fourier transform-infrared (FTIR) and differential scanning calorimetry (DSC) confirmed its structural integrity. The optimized (LRX-CS-LLCs) exhibited a particle size of 165.4 ± 6.3 nm, zeta potential of +26.3 ± 3.2 mV, and entrapment effectiveness of 98.2%. In vitro release followed a controlled kinetic profile. In vivo, LRX-CS-LLCs significantly reduced carrageenan-induced paw edema (77 ± 1.86% inhibition) and PGE2, COX-2, and TNF-α levels by 4.4-, 3.6-, and 3-fold, respectively, compared to the positive control group. Histopathological examinations confirmed normal tissue architecture. Notably, LRX-CS-LLCs outperformed pure-LRX, marketed-LRX, and uncoated-LRX-LLCs, emphasizing its promise as an effective oral therapeutic approach for enhanced management of inflammatory conditions.

**Keywords** Lornoxicam · Lipid carriers · Chitosan · Inflammation · Litsea cubeba · GC/MS

✉ Walaa A. El-Dakroury
walaa.ahmed2@buc.edu.eg

Abdelrahman R. Said
Abdelrahman.ragab@buc.edu.eg

Gihan F. Asaad
gihanfarag.ga@gmail.com

Heba M. I. Abdallah
hebam.i.abdallah@gmail.com

Marwa E. Shabana
marwashabana999@gmail.com

Rahma A. Abdelsalam
Rahmaabdelmotalib8@gmail.com

Eman M. Elsadek
emanelsadeq123@gmail.com

Basma H. Mohamed
basmahosam47@gmail.com

Yara S. Mohamed
roaasaeed467@gmail.com

Sara M. Seliem
saraseliem2012@gmail.com

Elsayed Y. Hamada
saiedyasser555@gmail.com

Belal W. Attef
belalattef54@gmail.com

Sara Saeed Kotb
sarah.kotb@buc.edu.eg

Shaza H. Aly
shaza.husseiny@buc.edu.eg

[1] Department of Pharmaceutics and Industrial Pharmacy, Faculty of Pharmacy, Badr University in Cairo (BUC), Badr City, Cairo 11829, Egypt

[2] Department of Pharmacology, Medical Research and Clinical Studies Institute, National Research Centre, Dokki, Cairo 12622, Egypt

[3] Pathology Department, National Research Centre, Dokki, Giza, Egypt

[4] Faculty of Pharmacy, Badr University in Cairo (BUC), Badr City, Cairo 11829, Egypt

[5] Department of Pharmacognosy, Faculty of Pharmacy, Badr University in Cairo (BUC), Badr City, Cairo 11829, Egypt

## Introduction

Oral route for drug administration is the most favored method for medicine delivery owing to its convenience, simplicity, and elevated patient adherence. In contrast to parenteral or transdermal routes, oral administration necessitates neither medical knowledge nor intrusive procedures, rendering it more acceptable to patients and appropriate for long-term treatment. The efficacy of oral medication delivery can be somewhat constrained when addressing medicines with low aqueous solubility. Poorly aqueous soluble medicines frequently have limited bioavailability due to restricted absorption in the gastrointestinal tract, resulting in unsatisfactory therapeutic effects.

Lornoxicam (LRX), a nonsteroidal anti-inflammatory drug (NSAID), one of the oxicam class, is frequently employed to modulate inflammation and control pain, demonstrating superior efficacy to other oxicams. It potently inhibits COX-1 and COX-2 enzymes, effectively alleviating inflammation and discomfort [1]. Despite its therapeutic advantages, lornoxicam poses hurdles when used orally. Prolonged usage of lornoxicam, like many NSAIDs, can cause gastrointestinal adverse effects, including peptic ulcers, potentially resulting in severe consequences. Moreover, owing to its brief half-life of around 3 h, frequent administration is necessary to sustain therapeutic concentrations. Lornoxicam's categorization as BCS Class II (low solubility with high permeability) exacerbates its oral administration, impeding its absorption [2]. To address these limitations, various nanoparticle-based delivery systems have been explored to enhance lornoxicam's oral delivery and bioavailability. Polymeric nanoparticles [3, 4], nanocrystals [5], nanosuspensions [6], solid lipid nanoparticles [7], self-nanoemulsifying systems [8], and nanoemulsions [9] have demonstrated potential in enhancing drug stability and facilitating controlled release. However, these systems possess inherent constraints, including restricted drug loading capacity, possible instability, and intricate production processes.

Lipid-based nanoparticles, especially nanostructured lipid carriers (NLCs), represent some of the most promising techniques for enhancing the oral delivery of lornoxicam. NLCs provide benefits compared to conventional SLNs by integrating a combination of solid and liquid lipids, leading to a more amorphous configuration [10]. This arrangement increases drug loading capacity, inhibits drug ejection, and facilitates sustained drug release, enhancing bioavailability and extending therapeutic benefits [11]. The diverse lipid matrix of NLCs improves the solubility and bioavailability of poor aqueous-solubility drugs such as lornoxicam [12].

The selection of liquid lipids (oils) in NLC formulations can affect the drug release profile and provide further therapeutic advantages. Many investigations were conducted to exploit the impact of different liquid lipids incorporation to enhance the loading capacity and efficacy of LRX but all these investigations utilized synthetic oils in the formulations [13, 14]. Litsea cubeba oil is especially beneficial as a liquid lipid due to its intrinsic anti-inflammatory effects. This oil, derived from the seeds and fruits of the *Litsea cubeba* plant, is recognized for its unique fragrant characteristics and extensive therapeutic advantages. Its significant medical property is its anti-inflammatory impact, owing to the oil's many bioactive components, including citral, limonene, and linalool. These chemicals demonstrate considerable anti-inflammatory and pain-killing action by inhibiting proinflammatory cytokine production and modulating oxidative stress. Litsea cubeba oil's anti-inflammatory properties render it a significant element in conventional and modern medicine for managing inflammation-related disorders. Incorporating Litsea cubeba oil into the NLC formulation (LLCs) not only enhances lornoxicam's solubility and entrapment effectiveness but also augments its therapeutic efficacy through a synergistic anti-inflammatory effect. This dual mechanism can enhance the overall effectiveness of treatments aimed at pain and inflammation, rendering it especially advantageous in formulations for NSAIDs such as lornoxicam [15, 16].

Furthermore, coating LLCs with biocompatible polymers like chitosan (CS) can provide additional benefits. CS, a natural cationic polymer, is produced via partial deacetylation of chitin. CS possesses numerous advantageous characteristics, encompassing mucoadhesive qualities, biocompatibility, and biodegradability. The surface modification of nanocarriers with CS has conferred multiple advantages, such as increased stability, prevention of drug leakage, extended drug release, enhanced mucoadhesion of nanoparticles, and augmented cellular uptake [17]. The electrostatic attraction linking the positively charged $NH_2$ groups of the CS and the negatively charged surface of the nanocarriers facilitates the coating process. In addition, CS alleviates the ant-inflammatory impact by inhibiting the synthesis of proinflammatory cytokines [18]. Furthermore, the chitosan-based coating demonstrated significant targeting capability for inflamed regions [19]. Various chitosan-surface modified nanoparticles have been documented for enhanced inflammation treatment. Examples comprised chitosan-coated Au-nanoparticles [19], chitosan-coated nanoemulsion [20], and chitosan-coated SLNs [21].

Integrating NLCs with Litsea cubeba oil (LLCs) offers a novel method for enhancing the oral administration of lornoxicam. Furthermore, chitosan coating improves the interaction of the LLCs with the gastrointestinal mucosa, promoting enhanced absorption and extended retention duration, hence aiding in controlled drug release and increased bioavailability. This combination mitigates the drawbacks of limited aqueous solubility, frequent dosing,

and gastrointestinal side effects while augmenting the medication's anti-inflammatory efficacy and bioavailability.

We aim to develop and optimize lornoxicam-loaded Litsea cubeba lipid carriers (LRX-LLCs), further coated with chitosan (LRX-CS-LLCs), in order to enhance oral efficacy, provide sustained release, and improve anti-inflammatory efficacy compared to conventional formulations.

## Materials and Methods

### Materials and Reagents

Litsea cubeba oil was purchased from Harraz Naturals (purity > 98%). Cetyl palmitate (CP) was acquired from Sigma Chemical Company (St. Louis, MO, USA), as well as Chitosan (CS) (medium M.W.). Tween® 80, ethyl alcohol, and phosphate buffer salts were obtained from El-Nasr Pharmaceutical Chemicals Company, Cairo, Egypt. Carrageenan (Carr; Sigma Aldrich, Germany). ELISA kits used: Prostaglandin E2 (PGE2; Cat.No.: ER1800, Wuhan Fine Biotech Co., Ltd., China), cyclooxygenase-2 (COX2; Cat. No.: DEIA6222, Creative Diagnostics, NY 11967, USA) and tumor necrosis factor-alpha (TNF-α; Cat. No. 438204, BioLegend, Inc., CA 92121, USA) as per the manufacturer's instructions. All chemicals utilized were of the highest industrial grade.

### Experimental Animals and Ethical Approval

Forty-eight adult male Wistar rats (150–180 g), were obtained from the animal breeding section at the National Research Centre. Established guidelines for optimum animal care include a normal light-dark cycle and the provision of adequately ventilated enclosures. The rats were accommodated in clean plastic enclosures and were given a consistent pellet diet, along with unrestricted access to water. Animal cadavers and tissue samples must be handled with strict adherence to cleanliness protocols; deceased specimens will be swiftly transferred to the Safety and Health Committee of the NRC following direct contact after euthanasia. All the experiments had been approved by the research ethical committee of Badr University in Cairo with approval number IACUC/PHA/155/A/2024.

### Methods

#### Gas Chromatography/Mass Spectrometry Assessment for Listea Cubeba Essential Oil

Gas chromatography/mass spectrometry (GC/MS) analysis was conducted using a Shimadzu GCMS-QP 2010 chromatograph (Kyoto, Japan) with a DB-5 capillary column. Column dimensions: 30 m × 0.025 cm inner diameter × 0.25 µm film breadth; Restek, USA. The temperature of the oven was maintained at 45 °C for 2 min (isothermal), then scheduled to decrease to 30 °C at a level of 5 °C/min, and held constant at 300 °C for 5 min (isothermal); the injector temperature was set at 250 °C. Helium was used as a transporter medium, with a flow rate established at 1.40 mL/min. Samples (1% v/v) were injected at a split ratio of 15:1, with an injection volume of 1 µL. The operational specifications for the MS were in this order: interface temperature: 280 °C, ion emitter temperature: 200 °C, EI mode: 70 eV, scan range: 35–500 amu. Identifying the oil components was conducted by analyzing their retention indices and correlating their mass spectra with the NIST-17 and Wiley library databases, in addition to published literature data [22–25]. Retention indices (RI) were computed with homologous series of n-alkanes (C8-C30) introduced under similar specifications.

#### Preparation of LRX -LLCs

LRX-loaded LLCs were developed via a heated homogenization technique, which was succeeded by sonication. The lipid portion, comprising solid and liquid lipid (CP and litsea oil, respectively), and LRX, was molten in a heating mantle at 65 °C. Afterward, thermally conditioned aqueous medium containing Tween® 80 as a surface active agent was subsequently included in the lipid blend with continuous homogenization at 17,000 rpm for 10 min utilizing a Homogenizer (Model 302, Mechanika Precyzyjna, Warszawa, Poland). Subsequent to homogenization, the mix was permitted to cool to ambient temperature and was subjected to sonication for 5 min utilizing a Branson Sonifier (250 W/102 C, Danbury, CT, USA). Different ratios of CP to litsea oil (80:20, 70:30, and 60:40) and varying surfactant concentrations (1%, 2%, and 2.5%) were investigated for subsequent investigation [26].

#### Particle Diameter and Zeta Potential Assessment

Dynamic light scattering (DLS) analysis was conducted to evaluate the nanoparticles' hydrodynamic diameter, polydispersity index (PDI), and surface charge. Before measurement, samples were diluted adequately with ultrapure water (HPLC grade) to achieve optimal scattering intensity and subjected to bath sonication (10 min, 40 kHz) to ensure colloidal dispersion. Freshly prepared suspensions were analyzed using a Zetasizer Nano ZS instrument (Malvern Panalytical, UK) at backscatter detection (173°). All measurements were conducted in three replications at 25 ± 0.5 °C, with the instrument calibrated using standard

latex dispersions. The reported values represent intensity-weighted distributions derived from cumulative analysis of three consecutive runs per sample, ensuring statistical reliability of the colloidal characterization data [27–29].

### Entrapment Effectiveness Evaluation (EE%)

The efficacy of entrapment (EE%) in LRX-LLCs was evaluated using an established indirect methodology. Freshly prepared LRX-LLC suspensions were exposed to ultracentrifugation at 20,000 rpm for 30 min at controlled temperatures using a refrigerated centrifuge (Hanil Scientific Inc., Korea), facilitating the separation of the nanoparticle from the supernatant containing unencapsulated drug [30]. The free LRX concentration in the supernatant was quantified via UV-Vis spectrophotometry (UV-160 A, Shimadzu, Japan) at a wavelength of 363 nm. Entrapment effectiveness was calculated using the formula:

$$EE\% = \frac{Total\ LRX\ amount - un\ entrapped\ LRX\ amount}{Total\ LRX\ amount}$$

### Optimization Data Assessment

A three-level factorial design ($3^2$) was implemented to thoroughly optimize LRX-CS-LLCs, incorporating two independent variables: the mass ratio of solid lipid (CP) to liquid lipid (Litsea oil) ($X_1$) and the concentration of Tween® 80 ($X_2$). The experimental matrix, comprising nine formulation variants, was executed to evaluate the influence of these factors on essential quality attributes, including particle size (PS), PDI, zeta potential, and EE%. Response data (Table 1) were analyzed using Design-Expert® software (v11, Stat-Ease Inc., USA), with one-way analysis of variance (ANOVA) applied to assess statistical significance ($\alpha = 0.05$). The model adequacy was verified through residual analysis and coefficient of determination ($R^2 > 0.90$), ensuring robust optimization of lipid nanoparticle characteristics. This systematic approach identified factor interactions governing colloidal stability and facilitating the development of LRX-CS-LLCs with tailored physicochemical properties for enhanced therapeutic delivery.

### Fourier Transform (FT-IR) Infrared Spectroscopy

The molecular interactions and structural integrity of LRX-pure (CP), Litsea oil, Tween® 80, plain LLCs, and optimized LRX-LLCs were investigated using a Bruker ALPHA II FTIR spectrometer (Bruker AXS GmbH, Germany) equipped with a diamond attenuated total reflectance (ATR) accessory. Spectral data were acquired in the mid-infrared range (4000–400 $cm^{-1}$) at a resolution of 4 $cm^{-1}$ across 32 scans to optimize signal-to-noise ratios. Before analysis, background scans of the ATR crystal were subtracted using Bruker OPUS 5.5 software, followed by baseline correction and vector normalization to minimize instrumental artifacts. Distinct vibrational bands were identified for each component [31].

### Differential Scanning Calorimetry (DSC)

The thermal performance of LRX-pure, CP, Litsea oil, Tween® 80, plain LLCs, and the optimized LRX-loaded LLCs was systematically investigated using differential scanning calorimetry (DSC) (Model Q200, TA Instruments, New Jersey, USA). Before analysis, the DSC system was calibrated with indium and zinc standards to ensure heat flow and temperature measurement accuracy. Approximately equal quantities of each sample were weighed into aluminum crucibles, hermetically sealed, and mounted on the instrument, with an empty crucible used as the reference. The thermal scans were performed over a 25 to 300 °C range, applying a consistent heating rate of 10 °C/min under a nitrogen atmosphere flowing at 20 mL/min. This procedure enabled precise assessment of phase transitions and thermal stability across all samples [32].

### Preparation of LRX-CS-LLCs

A chitosan solution (CS) 0.5% (w/w) was formulated by dispersing the requisite quantity of chitosan in 1% acetic

**Table 1** LRX-LLCs and their size, PDI, zeta potential, and entrapment effectiveness results

| Formula | LRX (mg) | Solid-to-liquid lipid ratio | Tween® 80% | Size (nm) | PDI | Zeta potential (mV) | EE % |
|---|---|---|---|---|---|---|---|
| F1 | 36 | 80:20 | 1% | 177.45 ± 4.7 | 0.296 | −24.4 ± 2.1 | 90.4 ± 4.2 |
| F2 | 36 | 80:20 | 2% | 114.31 ± 3.6 | 0.318 | −19.3 ± 1.6 | 88.7 ± 3.4 |
| F3 | 36 | 80:20 | 2.5% | 187.5 ± 7.2 | 0.279 | −17.71 ± 1.2 | 97.8 ± 3.7 |
| F4 | 36 | 70:30 | 1% | 134.5 ± 5.1 | 0.287 | −21.5 ± 1.7 | 97.9 ± 2.8 |
| F5 | 36 | 70:30 | 2% | 106.1 ± 6.7 | 0.239 | −19.2 ± 1.8 | 97.1 ± 3.4 |
| F6 | 36 | 70:30 | 2.5% | 144.1 ± 3.2 | 0.197 | −15.5 ± 0.9 | 95.76 ± 5.2 |
| F7 | 36 | 60:40 | 1% | 133.8 ± 2.9 | 0.259 | −20.3 ± 1.6 | 97.8 ± 6.1 |
| F8 | 36 | 60:40 | 2% | 84.01 ± 4.5 | 0.189 | −17.8 ± 0.8 | 98.2 ± 4.6 |
| F9 | 36 | 60:40 | 2.5% | 97.18 ± 7.4 | 0.387 | −14.5 ± 1.1 | 96.4 ± 2.9 |

*LRX*; lornoxicam, *PDI*; polydispersity index, and *EE*; entrapment effectiveness. Data are expressed as mean ± SD ($n = 3$)

acid and left on the stirrer overnight. The solution was subsequently filtered to eliminate any unincorporated CS particles. An equivalent quantity of CS solution was gradually introduced drop by drop into the LLC suspension and agitated for 24 h to acquire the coated LLCs [33].

### Morphology, Particle Diameter, and Zeta Potential for LRX-CS-LLCs

The diluted LRX-CS-LLCs underwent transmission electron microscopy (JEM-2100, JEOL, Japan) to evaluate their morphology. A small sample layer was applied to a copper grid, subjected to 1% phosphotungstic acid staining, and photographed for analysis. Particle size was also confirmed by DLS, in addition to PDI and zetapotential.

### In vitro Release of LRX

The dialysis bag procedure was retained to examine the release characteristics of LRX from optimized LRX-LLC and LRX-CS-LLCs formulations. Cellulose tubular membranes with a M.WT cutoff of 12,000 Da (Sigma Aldrich, St. Louis, MO) were accustomed by immersion in filtered water for 24 h before the investigation. The dialysis bags were fastened at the base with a brace and packed with 2 mL of the tested preparation (1 mg LRX). A subsequent clamp was employed to secure the tops of the bags. The bags were immersed in 200 mL of simulated gastric fluid (SGF) containing 0.1 N hydrochloric acid (HCl) at pH 1.2 for two hours. Subsequently, they were adjusted to SIF phosphate-buffered saline (PBS) at a pH of 6.8 and preserved at 37 °C ± 0.5 °C for 24 h. The vessels containing dialysis bags filled with the release media were tightly closed and positioned in a small thermostatic shaking incubator (BJPX-200 N, Biobase Co., China), operating at 80 rpm and maintained at 37 °C for the duration of the experiment [26]. At designated time intervals (0.5, 1, 2, 3, 4, 5, 6, 8, and 24 h), 2 mL aliquot was taken out from the release medium at predetermined intervals and immediately replaced with an equal amount of fresh medium to preserve sink circumstances throughout the study. The samples underwent spectrophotometric examination at a wavelength of 363 nm. The cumulative amount of LRX released was determined and plotted vs. time to generate a release profile. To gain deeper insight into the LRX release mechanism, the release behaviors of both coated and uncoated designated LLC formulations were analyzed using various kinetic models. The suitability of each model in describing the release pattern was evaluated by calculating the correlation coefficient ($R^2$), with higher values indicating a stronger fit to the predictive model.

### Mucoadhesion Studies

The mucoadhesive characteristics of LRX-CS-LLCs were assessed through their contact with mucin, utilizing particle size measurement and a turbidimetric analysis. For size assessment, equal quantities of mucin solution (0.5 mg/mL) and the preparation were combined, incubated, and subsequently examined for particle size and zeta potential via dynamic light scattering (DLS). In the turbidimetric analysis, mucin was solubilized in acetate buffer (pH 4.5), subjected to sonication, filtered, and subsequently combined with the formulation at different volume ratios (1:1, 2:1, 4:1). The mixes were incubated, and turbidity was quantified at 500 nm via UV spectrophotometry. The level of interaction was evaluated by contrasting the experimental absorbance with the theoretical cumulative absorbance of mucin and the formulation.

### Carrageenan-Induced Rat Paw Edema

Forty-eight male adult Wistar rats (150–180 g) were randomly allocated into six groups each of 8 animals. Group 1 functioned as the negative control and received no treatment. Group 2: A positive control was subcutaneously injected with 0.1 ml carrageenan (1% w/v) in the left hind paw [34]. Groups 3 and 4 were administered 9 mg/kg of pure-Dg and marketed-Dg orally [7, 35]. Group 5 received an administration of the plain optimized formula CS-LLCs at a dosage of 1 ml per rat. Group 6 received LRX-CS-LLCs at a 9 mg/kg dosage via oral administration. All forms of lornoxicam (LRX) and the plain formula (CS-LLCs) were orally administered 30 min before the induction of inflammation via carrageenan (1% w/v) [2] Paw thickness of all rats was measured with an MNT-150 vernier caliper (Jiangsu Goldmoon Industry Co., Ltd.- Shanghai, China) after carrageenan injection at 1, 2, 3, and 4 h, with results reported in millimeters [36, 37]. The edema and inhibition rates were calculated at the designated intervals using the following equations (38). Edema rate (%) = Tt - To/To, Inhibition rate (%) = Ec - Et/Ec.

where:

To the thickness before carrageenan injection (mm).
Tt the thickness at t hours after carrageenan injection (mm).
Ec the edema rate of the control group.
Et the edema rate of the treated group.

Blood samples were obtained from the retro-orbital plexus of overnight-fasted rats four hours after the administration of a 1% carrageenan injection. The animals were anesthetized with mild dosages of ketamine. Blood samples were centrifuged at 1500 x g for 10 min at 4 °C. The sera were

preserved at −80 °C until the evaluation of PGE2, COX2, and TNF-α inflammatory cytokines was conducted.

### Assessment of Inflammatory Cytokines

ELISA kits were used to quantify PGE2, COX2, and TNF-α concentrations, adhering to the manufacturer's guidelines. All metrics were assessed at an optical density of 450 nm.

### Gross Appearance and Histopathological Studies of Rats' Paws

Animals were humanely euthanized using an intraperitoneal injection of ketamine (80 mg/kg) combined with xylazine (10 mg/kg), then paw samples were excised from all groups, washed with normal saline, and grossly examined. Bone tissue was decalcified via immersion in a 10% EDTA solution for 30 days. The specimens were then preserved for a minimum of 72 h in 10% neutral-buffered formal saline. All specimens were washed under running water for 30 min, and then followed by dehydration, xylene clearing, and paraffin embedding. Serial slices with a thickness of 5 µm were produced and stained with hematoxylin and eosin (Drury and Wallington, 1980) for histological analysis. Images were acquired and processed using Adobe Photoshop version 8.0 [38].

### Statistical Analysis

The experimental optimization of formulations was systematically performed using Design-Expert® software (v11, Stat-Ease Inc.) through the surface response method to evaluate the multivariate effects of critical process parameters on key pharmaceutical qualities. Statistical significance of individual factor effects was determined via one-way ANOVA ($\alpha = 0.05$), with all experimental data reported as mean ± SD and 95% confidence intervals to ensure rigorous parameter estimation. For biological assessments, in vivo data were analyzed using GraphPad Prism® (v8.0) employing one-way ANOVA followed by tukey kramer's test for confirmation.

## Results and Discussion

### Gas Chromatography/Mass Spectrometry Analyses for Listea Cubeba Essential Oil

The *Litsea cubeba* oil was explored employing GC/MS to recognize its chemical constituents, which is described in Table 2. The GC/MS investigation of the essential oil of *Litsea cubeba* recognized eighteen compounds, demonstrating about 98.87% of the total oil. The major recognized compounds were establish to be *α*-citral (47.56%), along with *β*-citral (26.86%) and *D*-limonene (14.00%). The oil principally comprised oxygenated monoterpenes (77.44%) and monoterpene hydrocarbons (18.52%). A GC chromatogram of the *Litsea cubeba* oil is presented in Fig. 1(I).

In agreement with our results, previous research on *Litsea cubeba* essential oil discovered that the prevalent constituents were limonene (23.14%) and citral (14%) [15]. Also, in a previous report, GC/MS evaluation of Litsea cubeba oil indicatesd that citral (63.75%) and limonene (7.38%) were the predominant constituents [39]. Another report showed the presence of both citral isomers as significant constituents, accounting for 78.7% and 87.4% of the essential oil of *Litsea cubeba* fruits distributed in China [40]. Regarding the activity of *Litsea cubeba* oil, a recent study revealed that its essential oil demonstrated potential anti-inflammatory properties by reducing TNF-α, IL-6, and IL-1β levels in the liver and intestine along with molecular docking study on its major constituent citral that showed strong affinity for IL-1β, IL-6, and TNF-α, producing anti-inflammatory effects via hydrogen bonding interactions [41]. Another study indicated that the *Litsea cubeba* essential oil possesses anti-inflammatory properties using egg albumin denaturation assay, where the fruit and leaf essential oil showed 82.21% and 81.49% inhibition using concentrations of 0.20 and 0.25 mg/mL, respectively [15].

### Particle Size and Zeta Potential Assessment

The stability of the hot emulsion formed during the preparation process is a key point that reflects the particle size of the nanostructured lipid carrier. The more stable emulsion solidifies after cooling to create a smaller particle size. Table 1 presents that all the prepared LRX-LLC showed acceptable nanosize range with superiority observed by increasing the oil ratio in lipid composition. Also, surfactant concentration was observed to influence the particle size significantly. By increasing surfactant concentration (1 to 2%), the particle size decreased as observed between F1 vs. F2 (177.45 and 114.31 nm, respectively), F4 vs. F5 (134.5 and 106.1 nm, respectively), and F7 vs. F8 (133.8 and 84 nm, respectively). This is the acceptable trend as increasing the surfactant concentration leads to stabilization of the intermediate emulsion by distribution along the lipid/aqueous interface, decreasing the interfacial tension and preventing droplet aggregation [42, 43]. Further increase in surfactant concentration (2.5%) showed different behavior, which was 187.5, 144.1, and 97.18 nm for F3, F6, and F9, respectively, which was not expected. This could be assigned to the alteration in surface properties due to a higher level of accumulation of surfactants on the surface and bridging effects

**Table 2** Chemical composition (%) of *Litsea cubeba* essential oil using GC/MS analysis

| No. | Compound name | Formula | $R_t$ | Content % | $RI_{cal.}$ | $RI_{Lit.}$ | Chemical Class |
|---|---|---|---|---|---|---|---|
| 1 | *α*-Pinene | $C_{10}H_{16}$ | 7.09 | 1.84 | 929 | 935 | Monoterpene Hydrocarbon |
| 2 | Camphene | $C_{10}H_{16}$ | 7.51 | 0.68 | 943 | 946 | Monoterpene Hydrocarbon |
| 3 | *β*- Pinene | $C_{10}H_{16}$ | 8.35 | 1.72 | 972 | 974 | Monoterpene Hydrocarbon |
| 4 | 6-Methyl-5-hepten-2-one | $C_8H_{14}0$ | 8.72 | 0.39 | 984 | 985 | Ketone |
| 5 | *p*-Cymene | $C_{10}H_{14}$ | 9.84 | 0.28 | 1021 | 1021 | Monoterpene Hydrocarbon |
| 6 | ***D*-Limonene** | $C_{10}H_{16}$ | 9.97 | **14.00** | 1025 | 1025 | Monoterpene Hydrocarbon |
| 7 | Linalool | $C_{10}H_{18}O$ | 12.19 | 1.28 | 1097 | 1097 | Oxygenated Monoterpene |
| 8 | 3,7-Dimethyl-3,6-octadienal | $C_{10}H_{16}O$ | 14.73 | 0.30 | 1180 | 1184 | Oxygenated Monoterpene |
| 9 | α-Terpineol | $C_{10}H_{18}0$ | 15.00 | 0.20 | 1189 | 1189 | Oxygenated Monoterpene |
| 10 | *cis*-Geraniol | $C_{10}H_{18}0$ | 16.14 | 0.31 | 1227 | 1228 | Oxygenated Monoterpene |
| 11 | ***β*-Citral** | $C_{10}H_{16}0$ | 16.54 | **26.86** | 1241 | 1241 | Oxygenated Monoterpene |
| 12 | Piperitone (3-Carvomenthenone) | $C_{10}H_{16}0$ | 16.91 | 0.69 | 1254 | 1254 | Oxygenated Monoterpene |
| 13 | ***α*-Citral** | $C_{10}H_{16}O$ | 17.44 | **47.56** | 1272 | 1271 | Oxygenated Monoterpene |
| 14 | Geranic acid | $C_{10}H_{16}O_2$ | 20.01 | 0.24 | 1363 | 1355 | Oxygenated Monoterpene |
| 15 | *trans*-*β*-Caryophyllene | $C_{15}H_{24}$ | 21.54 | 1.35 | 1419 | 1419 | Sesquiterpene Hydrocarbon |
| 16 | *α*-Caryophyllene (*α*-Humulene) | $C_{15}H_{24}$ | 22.44 | 0.21 | 1454 | 1454 | Sesquiterpene Hydrocarbon |
| 17 | Caryophyllene oxide | $C_{15}H_{24}O$ | 25.77 | 0.76 | 1585 | 1585 | Oxygenated Sesquiterpene |
| 18 | Neric acid | $C_{10}H_{16}O_2$ | 37.54 | 0.20 | 2140 | 1374 | Oxygenated Sesquiterpene |
| Total identified compounds % | | | | **98.87** | | | |
| Monoterpene Hydrocarbons % | | | | **18.52** | | | |
| Oxygenated Monoterpenes % | | | | **77.44** | | | |
| Sesquiterpene Hydrocarbons % | | | | **1.56** | | | |
| Oxygenated Sesquiterpenes % | | | | **0.96** | | | |
| Others | | | | **0.39** | | | |

promoting aggregation. Other investigators witnessed this observation of increased particle size beyond specific surfactant concentrations and similarly explained [44–46]. In contrast, changing the solid-to-liquid lipid ratio showed a universal trend of decreasing particle size upon increasing the liquid lipid ratio at each surfactant concentration (Table 1). This was expected and can be ascribed to the fact that liquid lipid tends to decrease the viscosity of lipids during homogenization, which allows free adsorption of surfactant molecules on the droplet interface before solidification [47]. Also, decreasing solid lipid composition reflected smaller particle size [48]. All prepared formulations ' polydispersity index (PDI) values showed an acceptable homogeneity range (Table 1). However, all formulations were at the same level of size distribution without significant superiority.

Zeta potential values of the prepared LRX-LLC showed a clear trend of zeta potential decrease with increasing surfactant concentration (Table 1). This is ideal, primarily since Tween® 80 is known as a nonionic surfactant; the reduction of particles' surface potential can be elucidated by the ability of surfactant molecules to displace the surface fatty molecules due to the advanced surface action of Tween® 80 [49]. As surfactant molecules are nonionic while the original surface fatty molecules are anionic, the total decrease in particle zeta potential can be explained. Other researchers have reported a similar trend for Tween® 80 [42].

## Entrapment Effectiveness Determination

The values of the percentage of entrapped LRX in the tested formulations are listed in Table 1**.** All tested formulations showed high effectiveness in entrapping LRX (88.7 to 98.2%) Regarding the solid-to-liquid lipid ratio, formulations with the low contribution of liquid lipid showed remarkably inferior results compared to corresponding formulations with higher liquid lipid contribution, which reflected the impact of Litsea oil incorporation in improving LRX entrapment in the prepared formulations. This was expected as LRX is relatively more soluble in this liquid lipid than solid lipid, and formulations with high liquid lipid composition showed smaller particle size, allowing more surface area for LRX partitioning during the preparation. However, a further increase in the liquid lipid in lipid composition did not show noticeable enhancement, which suggested 70:30 as the optimum solid-to-liquid lipid ratio [50]. Increasing the percentage of the surfactant showed only a trend of increased entrapment effectiveness, especially in formulations with low liquid lipids (Table 1). This was expected as surfactants can improve the LRX partitioning to the oil compartment during preparation [51]. However, this behavior showed less impact in formulations with high liquid lipids, where the highest surfactant percentage (2.5%) reported inferior entrapment effectiveness, which

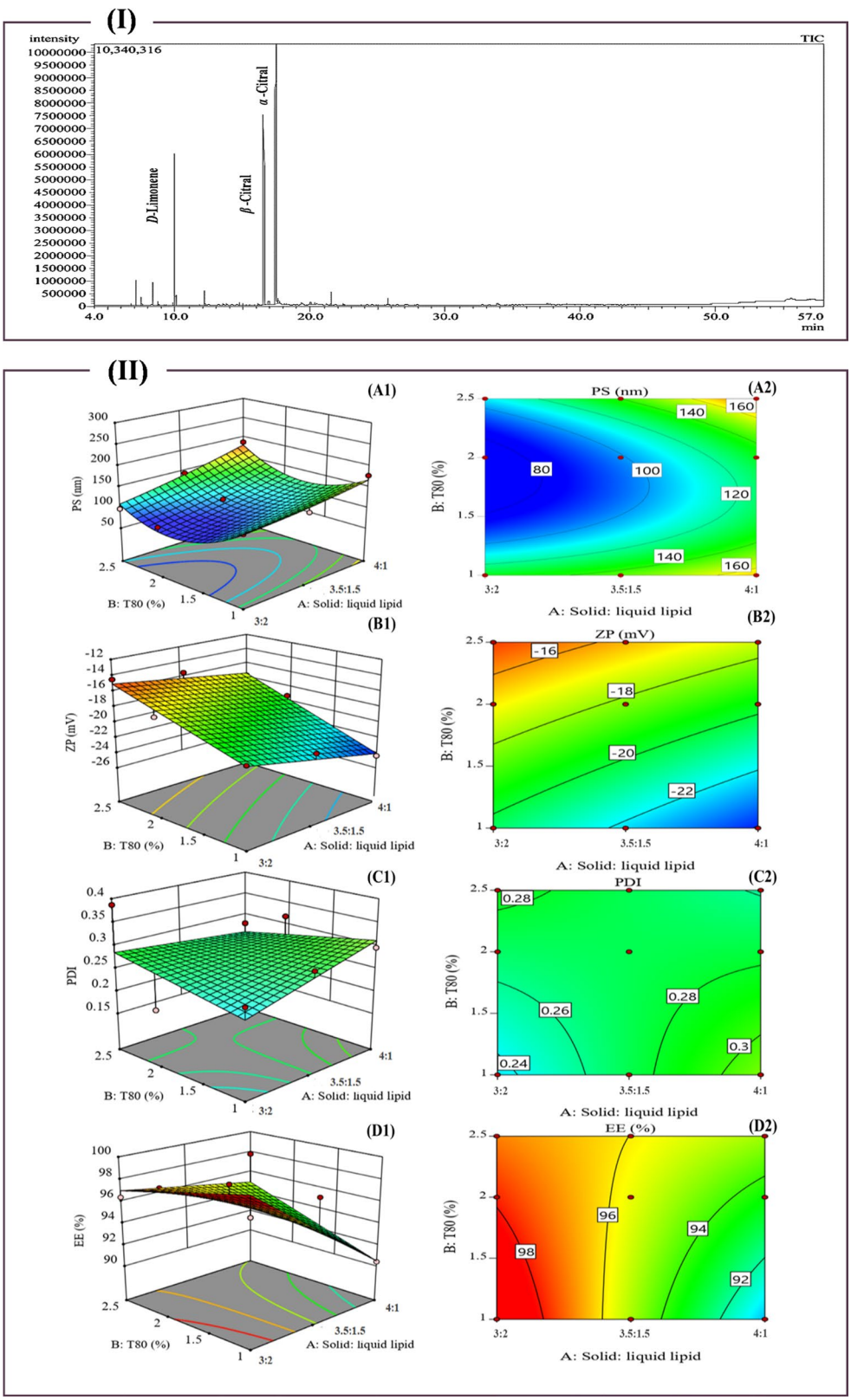



**Fig. 1** (I) GC chromatogram of the essential oil of *L. cubeba* with its major constituents. Figure 1 (II) 3-D response and Contour diagram demonstrating the influence of solid-to-liquid lipid proportion and surfactant concentration in LRX-CS-LLCs on particle dimension (A1 & A2), zeta potential (B1 & B2), PDI (C1 & C2), and entrapment effectiveness percentage (D1 & D2)

was unexpected. This can be attributed to the ability of surfactants in high concentration to form micelles entrapping liquid lipids within the formulation, which influences its ability to entrap LRX to the expected level [52].

## Optimization Data Assessment

The potential influence of the solid-to-liquid lipid proportion and surfactant percentage on the particle diameter of the LRX-LLCs was illustrated by a contour graph and surface response **(Fig. 1II A1&A2).** The following polynomial equation can explain it.

$$PS = 98.71 + 29.44 * A + 39.57 * B + 12.38 * AB + 4.14 * A^2 + 86.68 * B^2.$$

Where A represents the solid-to-liquid lipid ratio and B represents the surfactant concentration. This coded equation can predict particle size at different factor levels (high levels coded as +1 and low levels as −1). The coefficients indicate the relative impact of each factor: the positive values for A and B show that increasing either factor leads to an increase in particle size. In contrast, the significant coefficient of $B^2$ demonstrates that surfactant concentration has a more substantial quadratic effect on particle size than lipid ratio. The interaction term (AB) further suggests that the combined impact of lipid ratio and surfactant concentration contributes significantly to the variation in particle size.

It was proposed that both variables affected the particle size. The greatest particle diameter was noted with an increased percentage of Tween® 80 and a solid lipid-to-liquid lipid ratio of 80:20. Increasing the concentration of Tween® 80 from 1% to 2% reduced the size; however, raising it from 2% to 2.5% significantly increased the size. Previous investigations indicated that certain surfactant compounds can raise localized osmotic pressure at increased surfactant concentrations. This results in the migration of the external phase across certain droplets, causing a depletion of the aqueous phase among droplets. Consequently, aggregation takes place, leading to a boost in particle size [53]. Furthermore, there might be a point at which the surfactant molecules begin to cluster or form micelles instead of maintaining a uniform distribution around the lipid particles. This may guide to the formation of bigger aggregates, thereby augmenting the overall particle size of the LLCs [42]. Tween® 80 is a surfactant designed to enhance the stability of LLCs by reducing the tension in the interface between their lipid and aqueous phases; however, excessive amounts of Tween® 80 can result in particle aggregation, hence enlarging the particle size. Another justification suggests that Tween® 80 can enhance the viscosity of the preparation. Elevated viscosity can impede the movement of lipid particles throughout homogenization, resulting in impaired size reduction efficiency and, perhaps, higher final particle dimensions [54]. Accordingly, greater surfactant concentration compared to a lipid ratio results in smaller particles. Conversely, elevating surfactant concentrations beyond a specific threshold increases particle size [55].

The solid lipid-to-liquid lipid content significantly affected the optimum particle size of LRX-LLCs. Increased quantities of solid lipids typically lead to an augmentation in the particle diameter of LLCs. The rationale for this phenomenon is that solid lipids, owing to their increased stiffness, facilitate the creation of larger particles during the cooling down and solidification process. A study demonstrated that increasing the solid-to-liquid lipid proportion produced particle sizes between 150 and 281 nm, contingent upon the exact ratio utilized [56]. Conversely, increasing the proportion of liquid lipids in lipid-based formulations has been shown to reduce particle size, a phenomenon attributed to enhanced emulsification efficiency driven by alterations in the lipid phase's thermodynamic properties. The incorporation of liquid lipids lowers the melting point and increases the fluidity of the lipid matrix, which facilitates finer dispersion during homogenization and promotes the formation of smaller, more monodisperse droplets. This effect is further stabilized during solidification, yielding LLCs with reduced particle dimensions and a homogeneous size distribution. Empirical studies have consistently demonstrated a direct correlation between elevated liquid lipid content and the generation of smaller, more uniform particles [57].

Both parameters manipulated the zeta potential, as proven in the contour chart and surface response (Fig. 1II B1&B2). The following polynomial equation can explain it.

$$ZP = -18.25 + 1.4 * A - 3.99 * B + 0.44 * AB.$$

The positive coefficient of A indicates that increasing the proportion of solid lipid increases the zeta potential, while the negative coefficient of B shows that increasing surfactant concentration diminishes the surface charge. Elevating Tween® 80 concentration from 1% to 2.5% diminished the zeta potential of LLCs. This reduction arises from Tween® 80's nonionic nature, which eliminates surface charges while sterically stabilizing particles. Tween® 80 predominantly facilitates steric stabilization over electrostatic stabilization, and at elevated concentrations, the equilibrium between these effects alters, potentially affecting overall dispersion stability [42, 54, 58]. Increased liquid lipid concentration could affect the structural integrity of the LLCs. An enhanced fluidity of the matrix may diminish electrostatic repulsion among particles, resulting in a diminished effective zeta potential when particles approach one another and interact more intensely, perhaps neutralizing a portion of surface charges [51]. Moreover, elevated liquid lipid ratios

typically yield smaller particle sizes owing to enhanced emulsification and diminished viscosity during formulation. Smaller particles may demonstrate reduced absolute zeta potentials due to their increased surface area relative to volume, influencing the distribution of charges across their surfaces [59]. Additionally, including surfactants in LLC formulations is crucial for stabilizing the particles. As the concentration of liquid lipids rises, surfactants may exhibit diminished efficacy in delivering steric stabilization due to alterations in their interactions with both solid and liquid lipids. This reduction in stability may also result in a drop in zeta potential [60].

The PDI was explained by the was following polynomial equation

$$\mathrm{PDI} = 0.2722 + 0.0039 * \mathrm{A} - 0.0006 * \mathrm{B} - 0.0349 * \mathrm{AB}$$

The equation shows that the coefficients of the individual factors (*A* and *B*) are very small, indicating that both factors are statistically non-significant in influencing PDI. However, the interaction term (*AB*) has a larger negative coefficient, showing that the combined effect of lipid ratio and surfactant concentration reduces PDI and improves uniformity. Especially, a 2% Tween® 80 and a diminished ratio of solid lipid to total lipid enhanced particle diameter homogeneity and decreased the PDI value, as illustrated in the contour chart and surface response (Fig. 1II C1&C2)**.** A comparable outcome was previously articulated [61].

EE was exclusively modulated by the solid-to-liquid lipid ratio, as demonstrated by the contour plot and response surface analysis (Fig. 1II D1&D2). The following polynomial equation can explain it.

$$\mathrm{EE} = 95.67 - 2.19 * \mathrm{A} + 6.35 * \mathrm{B} + 2.36 * \mathrm{AB}.$$

The negative coefficient of A indicates that increasing the solid-to-liquid lipid ratio tends to reduce EE, while the positive coefficient of B shows that higher surfactant concentration improves EE. The interaction term (AB) further demonstrates that the combined effect of both variables significantly influences EE.

A direct proportionality was observed between liquid lipid content and EE, indicating that higher liquid lipid concentrations enhance the capacity of the lipid matrix to encapsulate the active compound. This phenomenon may arise from the improved molecular mobility, flexibility, and interfacial fluidity conferred by liquid lipids, which likely optimize drug partitioning into the lipid phase and minimize expulsion during nanoparticle solidification. Studies have shown that the efficacy of entrapment of raloxifene and quetiapine fumarate increased with higher liquid lipid concentrations in formulations [62]. Furthermore, elevated ratios of liquid lipids typically result in reduced particle sizes owing to enhanced emulsification and dispersion during the formulation process. Diminished particle dimensions yield an increased surface area relative to volume, facilitating improved interaction between the drug and the lipid matrix, thus augmenting the effectiveness of entrapment. Studies indicate that an increase in liquid lipid content correlates with a decrease in particle size, which is advantageous for sustaining elevated entrapment levels [63]. Conversely, an increase in the amount of solid lipids results in a more rigid lipid matrix, which may diminish the capacity of the LLC to encapsulate pharmaceuticals. This behavior has been observed in formulations where a higher concentration of solid lipids reduces the available space for drug incorporation inside the matrix [64].

The desire factor approach, a statistical technique, enhanced formulations by concurrently assessing many response characteristics. This method transforms every result parameter into a desirability value ranging from 0 (meaning total unfavorable) to 1 (signifying high preference) through specific desire functions. These functions relate to distinct response attributes: 'maximization' for characteristics that ought to be elevated, such as zeta potential and entrapment efficacy; 'minimization' for characteristics that should be reduced, including particle size and PDI; and 'goal fulfilment' for variables that must attain a predetermined value. Upon transforming each response into its respective desirability significance, these values are aggregated into a singular score, typically utilizing the geometric mean. Optimization involves refining the formulation factors to enhance the whole appeal score. This ensures that the final formulation achieves the ideal equilibrium of all response variables. The choice of F8 was determined by its maximum attractiveness factor of 74.6% and was earmarked for additional evaluation.

## Fourier Transform Infrared (FTIR) Spectroscopy

The associations across the formulation's components were determined through FTIR investigation. The FTIR plot of LRX-pure (Fig. 2I, A) unveiled a distinctive peak at 3062 $cm^{-1}$ attributed to amino functional groups, pronounced spikes at 1643 $cm^{-1}$ associated with the carbonyl content, a prominent peak at 1594 $cm^{-1}$ related to amino twisting vibration, a pointy band at 1321 $cm^{-1}$ linked to the $SO_2$ group, and a defined band at 781 $cm^{-1}$ referring to the C-Cl group [2, 7].

The FTIR of CP, illustrated in Fig. 2I, B, has several unique, distinctive peaks confined to the compound. The $CH_3$ and $C_2H_5$ groups display a pronounced spectrum of absorption at 2913 and 2847 $cm^{-1}$, respectively, correlated with the C-H symmetrical stretching trembling. A notable absorption peak at 1730 $cm^{-1}$ signifies the C = O stretching vibration in

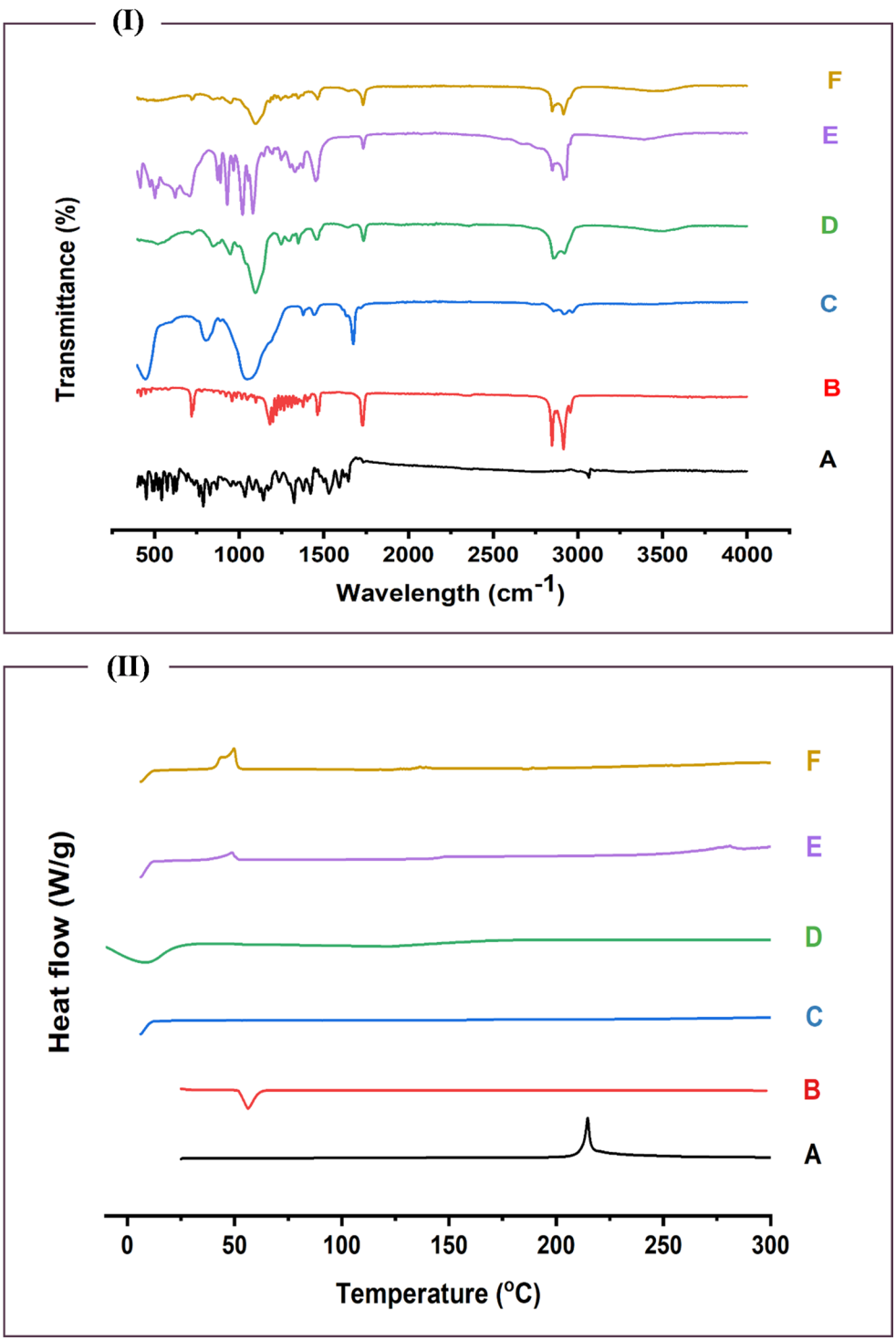



**Fig. 2** I. FTIR spectra of (A) LRX-pure, (B) CP, (C) Litsea oil, (D) Tween® 80, (E) plain LLCs, and (F) LRX-LLCs. Figure 2II. DSC thermogram of (A) LRX-pure, (B) CP, (C) Litsea oil, (D) Tween® 80, (E) plain LLCs, and (F) LRX-LLCs

the ester bond. A prominent absorption peak shows the C-H extension vibration in the $C_2H_5$ group at 1461 $cm^{-1}$, while a notable peak matches the in-plane stretching vibration of the O-H group at 718 $cm^{-1}$. CP also exhibits peak values at 1043 and 1182 $cm^{-1}$, signifying the prolonged vibrations of the carbonyl C = O group in the hexadecenoic acid hexadecanoate produced during the esterification step [21].

In Litsea Cubeba oil (Fig. 2I, C), a significant band was observed at 1673 $cm^{-1}$, corresponding to the C = O extension vibration of citral, the predominant component of the oil. The C = C bending frequency was observed at 1630 $cm^{-1}$. The bands observed at 1377 and 1441 $cm^{-1}$ were ascribed to limonene, a significant component of Litsea oil's chemical profile [65].

(Fig. 2I, D) presents the FTIR spectra of pure Tween® 80. The symmetrical and asymmetrical stretching vibrations of the methyl group result in absorption peaks at 1351 $cm^{-1}$ and 1455 $cm^{-1}$. A peak at around 3490 $cm^{-1}$ was observed in the FTIR spectrum of Tween® 80 for hydroxyl group stretching, at 2854 and 2919 $cm^{-1}$ for $CH_2$ and $CH_3$ stretching, respectively. A peak at 1092 $cm^{-1}$ for C-O-C was also observed, as were peaks at 1732.95 $cm^{-1}$ for C = O-stretching and 1630 $cm^{-1}$ for HOH-twisting. The FTIR chart of Tween® 80 was consistent with the documented data [66–68].

The spectrum of plain LLCs (Fig. 2I, E) displays distinct peaks correlated with the lipid and surfactant constituents (CP, Litsea Oil, and Tween® 80). No new peaks indicative of robust covalent bonds were detected; nevertheless, the existence of non-covalent contacts, including hydrogen bonding, is apparent from the spectrum shifts and peak broadening in the FTIR study. Hydrogen bonding is probable between the OH groups in Tween® 80 and the lipid carbonyl groups, as evidenced by the minor shifts and reduced intensity in the stretching vibrations of hydroxyl (-OH) and carbonyl (C = O) at approximately 3402 and 1735 $cm^{-1}$, respectively. A similar result was reported [69, 70].

The FTIR chart obtained from LRX-LLCs (Fig. 2I, F) exhibited similarity to those of the plain LLC structures (without LRX); this may be attributed to the trapped drug inside the lipid matrix, potentially obscuring drug-specific peaks in the FTIR spectrum. This occurs because the drug molecules are scattered at a molecular level within the lipid framework, limiting their visibility in the FTIR spectrum. This observation suggests that the integration of the drug did not alter the overall arrangement of the LLC excipients within the LLCs. Furthermore, it can be inferred that LRX was confined to the LLC [70, 71].

## Differential Scanning Calorimetry (DSC)

The DSC assessment offers essential insights into thermal behaviour, crystallinity, and interactions among excipients in pharmaceutical formulations.

Pure-LRX (Fig. 2II, A) displays a distinct exothermic peak at 214.5 °C in its DSC thermogram, signifying direct melting and destruction. This peak signifies its crystalline nature. Melting and thermal decomposition coincided with prior investigators, shown by an exothermic peak at 225 °C, typical of the crystalline stage [2, 72].

The thermal assessment of CP (Fig. 2II, B) reveals a singular melting endothermic peak at 56.47 °C, accompanied by an enthalpy of 146.7 j/g, signifying the existence of the β-polymorph state. This crystal is the utmost thermally stable crystal form of CP lipids. The results aligned with previously reported studies [21].

The finding of an exothermic peak at 170 °C in the DSC thermogram of Litsea oil (Fig. 2II, C) is noteworthy. This peak presumably signifies a chemical or physical transition occurring at this temperature. Litsea oil contains a high concentration of volatile chemicals, including citral (trans-citral and cis-citral) and d-limonene. At high temperatures (170 °C), certain chemicals may experience oxidation or thermal breakdown as oxygen from the atmosphere promotes the production of polar constituents, resulting in an exothermic process. This aligns with the thermal fragility of numerous essential oils at elevated temperatures. The exothermic peak may also arise from the decomposition of terpenes or other organic molecules in the oil, releasing energy [73, 74].

The DSC chart of Tween® 80 (Fig. 2II, D) displays a broad endothermic peak at 123.47 °C, corresponding to the flash point of the complicated blend of polyoxyethylene sorbitan and oleic acid esters, the principal constituents of Tween® 80, indicating the initiation of thermal degradation or volatilization [67, 75].

The DSC diagram of plain LLCs (Fig. 2II, E) exhibited a significant exothermic peak at 208 °C, accompanied by ΔH of 19.93 J/g, suggesting a potential interaction among Tween® 20 and Litsea oil. A subsequent transition peak occurs at 48.81 °C, accompanied by an enthalpy change of 21.95 J/g. This peak pertains to CP, the principal component of the LLC. The observed decrease in both the transition temperature and enthalpy of CP indicates a reduction in its crystallinity while enclosed within the nanoparticle. This result was observed for the CP excipients of LLC, as recorded in the literature [76].

The DSC curve of LRX-LLCs (Fig. 2II, F) exhibited an exothermic peak at 288.2 °C with ΔH of 25.82 J/g, akin to that of ordinary LLCs, though with a slight alteration in the melting point. A second peak was observed at 49.63 °C, with an associated ΔH of 66.29 j/g, corresponding to CP. Significantly, there was an absence of an exothermic peak related to the LRX melting point, indicating the total confinement of LRX inside the lipid matrix of the LRX-LLCs and the transformation of the LRX crystalline state into an amorphous state within the lipid matrix. The alteration of the LRX state may improve its bioavailability [76–78].

## Morphology, Particle Size, and Zeta Potential for LRX-CS-LLCs

CS (Medium MWT) was chosen to coat LRX-LLCs (F8) because of its ideal viscosity. Following the coating process, the particle size markedly increased from 84.01 ± 4.5 nm to 165.48 ± 6.3 nm, signifying the effective coating of the CS layer on the LLC surface. The zeta potential transitioned from a minus value of −17.8 ± 0.8 mV to a positive value of 26.32

± 3.2 mV, indicating the positive electrostatic characteristic of CS. This significant alteration in dimensions and surface potential offers compelling evidence for the successful coating of LLCs with CS. Comparable size and zeta potential findings were documented [79, 80]. Furthermore, transmission electron micrographs of the synthesized LRX-CS-LLCs (Fig. 3A) depict sphere-shaped particles with diameters in the nanometre range, with the highest frequency from 140 to 150 nm. The generated particles exhibited a uniform particle size, as the spotted histogram shows (Fig. 3B), which is confirmed by the low PDI value (0.214).

### *In vitro* LRX Release Profile

The release profiles of the coated (LRX-CS-LLCs) and uncoated (LRX-LLCs) formulations were plotted and

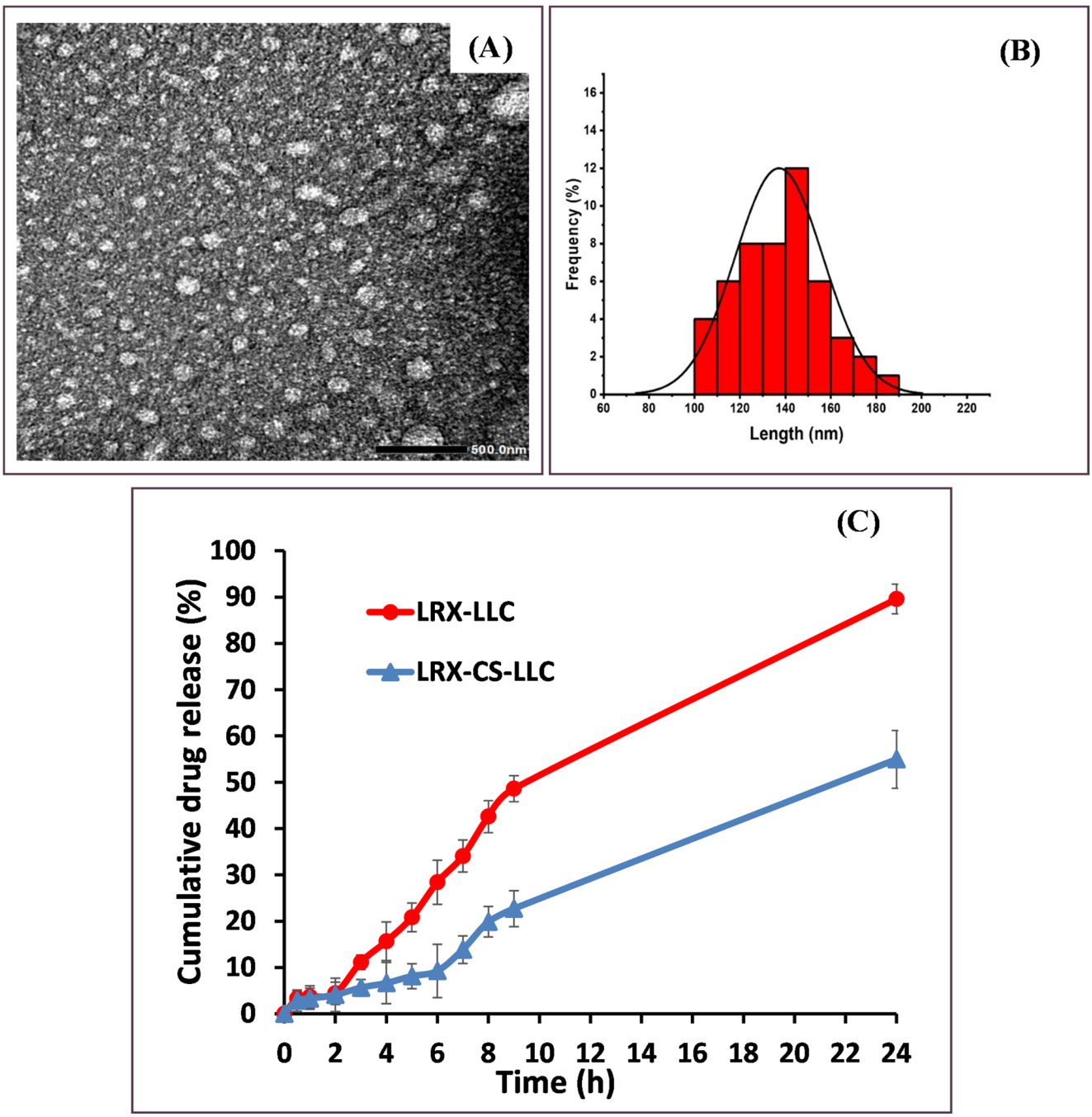



**Fig. 3** TEM picture of LRX-CS-LLCs (scale bar = 500 nm) (A), TEM distribution histogram depicting the particle dimension of LRX-CS-LLCs (B), and In vitro release of LRX from uncoated optimized formulation (LRX-LLC ●) and coated optimized formulation (LRX-CS-LLC ▲). (error bars represent ± SD)(C)

presented in Fig. 3C. The change in pH of the release medium shows mixed release behavior as two factors are affected by the pH change. The first is the solubility of LRX, which has been widely reported to be enhanced by increasing pH [81]. The other factor is the well-known pH-responsive behavior of CS, as it is soluble in low pH values (below 6.3) and present in a polycationic state, allowing the release of the entrapped drug. At the same time, its solubility decreases (gelling) at high pH (above 6.3), making a physical coat that controls the drug release [82, 83]. In Fig. 3C, the release of both coated and uncoated formulations was similar initially, where the release medium is acidic (4.1 and 4%, respectively, after 2 h). This was expected as LRX has poor dissolution in an acidic medium, besides the fact that the CS-coat is swollen, making it predictable to present release behavior similar to the uncoated formulation. By changing the pH, the coated and uncoated release behavior was expected to be increased as LRX has good dissolution in this medium. However, this was observed in the uncoated formulation (LRX-LLC), which showed an ideal release of particulate nanocarriers, showing 89.6% liberation of LRX after 24 h. On the other hand, the coated formulation (LRX-CS-LLCs) did not present remarkably enhanced drug liberation. It showed controlled release behavior with about 54.9% LRX liberation after 24 h, significantly different from the uncoated formulation's release profile (similarity factor, $f_2 = 48.4\%$). This was expected as the CS-coating layer undergoes gelling in this pH, which creates a barrier that prevents free drug release. Notably, this controlled release behavior of LRX-CS-LLC is favorable as it helps to protect the drug from unnecessary loss during GI absorption, delivering as much LRX as possible. Furthermore, the absorbed formulation is distributed passively to the inflamed area by the enhanced permeability retention (EPR) effect, where the pH is lower than the central circulation, allowing the release of LRX, specifically in inflammation sites [84]. Other investigations reported similar release behavior from chitosan coated nanoplatforms [85, 86]. It is important to note that exploiting EPR effect is special property for the absorbed intact particles after M cell endocytosis process which distribute the intact coated particles to the lymphatic vessels and then to the systemic circulation to be able to accumulate in the inflammatory sits [87].

The study of the release kinetics from coated and uncoated formulations also reflected significant controlled liberation of LRX from the coated formulation. This was reflected by the best fitting of the release profile of LRX-CS-LLC to zero-order release kinetics (Table 3). This can be attributed to the saturation of the CS layer with LRX, which acts as a barrier membrane against the liberation of the drug (rate-limiting step). Consequently, the release profile is purely representative of drug liberation from the saturated chitosan layer. Similar behavior was reported previously for CS-coated nanosystems [88]. Conversely, the release profile of the uncoated LLCs showed an ideal release mechanism as particulate nanoparticles. This best fits the Higuchi model, indicating diffusion-dependent release kinetics (Table 3). Notably, the mechanism of release of LRX from the uncoated formulation was affected by pH change, which was observed as a T lag period of around 2.85 h (equal to the time in the acidic release medium) before the Higuchi release model was initiated. By observing the release profile of the coated formulations, no T lag period can be calculated, and the release obeys the zero-order kinetic model in all pH conditions.

## Mucoadhesion Studies

Mucus in healthy persons predominantly comprises water, mucins, proteins, lipids, macromolecules, electrolytes, and microbes. Mucins, the principal glycoprotein constituent of mucus, are released by goblet cells and submucosal glands. These compounds exhibit a net negative charge at pH values exceeding 2.6, mainly attributable to the presence of sialic acid residues and ester sulfate groups. The negative charge of mucins facilitates their interaction with positively charged molecules. In the instance of LRX-CS-LLCs, CS imparts a positive surface charge via its protonated ammonium groups, enhancing these interactions.

The interaction between mucin and LRX-CS-LLCs was evaluated by comparing the nanoparticles' particle size and zeta potential before and after incubation with mucus. A notable augmentation in particle size was recorded after exposure to mucin, with the mean diameter escalating from 165.48 ± 6.3 nm to 389 ± 8.6 nm ($p < 0.05$) **(**Fig. 4A**)**. Additional proof of this connection was supplied by zeta potential testing. Mucin exhibited a negative surface charge (− 7.3 ± 0.4 mV). In contrast, the initial positive zeta potential of LRX-CS-LLCs (26.32 ± 3.2 mV) dramatically diminished to 6.7 ± 0.5 mV post-incubation ($p < 0.05$) **(**Fig. 4B**)**. The significant decrease in surface charge, along with the rise in particle size, robustly corroborates the electrostatic

**Table 3** Correlation coefficient ($R^2$) values after linear regression analysis of the LRX release profile of LRX-CS-LLC and LRX-LLC fitted to different release kinetics models

| Formulations | Zero-order | | First-order | | Higuchi | |
|---|---|---|---|---|---|---|
| | $T_{lag}$ | $R^2$ | $T_{lag}$ | $R^2$ | $T_{lag}$ | $R^2$ |
| *LRX-LLC* | −0.63 | 0.955 | 0.755 | 0.966 | **2.851** | **0.976** |
| *LRX-CS-LLC* | -- | **0.979** | -- | 0.944 | -- | 0.713 |

interaction between the negatively charged mucin and the positively charged nanoparticles [89].

Further validation of the mucin–NP interaction was achieved via turbidity studies, indicative of aggregation formation and particle development. A calibration curve was established to confirm the concentration-dependent nature of mucin absorbance, demonstrating a steady linear increase in absorbance with varying mucin concentrations. Turbidity assessments were performed at 500 nm utilizing UV spectrophotometry. The absorbance difference (ΔA) between the mucin–NP mixes and the theoretical sum of their separate absorbances was graphed against various mucin-to-NP ratios (Fig. 4C). All ΔA values were positive, signifying effective interaction, with increased absorbance differences noted at elevated mucin ratios, indicating improved binding affinity [89].

## Evaluation of the Impact of Lornoxicam in Various Formulations on Edema & Inhibition Rates and Cytokine levels (PGE2, COX-2, and TNF-α)

Carrageenan serves as a suitable model for evaluating the inflammatory mediators implicated in the induction of paw edema. The inflammation resulting from carrageenan sub-planter injection exhibits a biphasic response. Initially, histamine, serotonin, and bradykinin are released within the first hour, followed by a delayed phase attributed to the infiltration of polymorphonuclear leukocytes and the production of prostaglandins after one hour [90]. Following carrageenan injection, other mediators such as prostaglandin, thrombin, and reactive oxygen species (ROS) are released [91]. Common signs of local inflammation, including redness, swelling, fever, discomfort, and loss of tissue function, result from the interplay of various inflammatory mediators and components [92]. A strong relationship was observed between carrageenan-induced edema and prostanoid synthesis and their expression at the site of peripheral inflammation. Prostaglandin E2 (PGE2) levels are elevated during both phases of inflammation and show a progressive increase over time [93]. PGE2 is believed to be a key factor in initiating and regulating the inflammatory process, alongside tumor necrosis factor-α (TNF-α) [94]. Cyclooxygenase-2 (COX2) is the primary enzyme involved in the biosynthesis of PGE2, facilitating the conversion of arachidonic acid to PGE2 [95]. Furthermore, numerous inflammatory diseases are markedly affected by the COX-2/PGE2 pathway. Prior experimental results have validated the essential function of this pathway in the anti-inflammatory

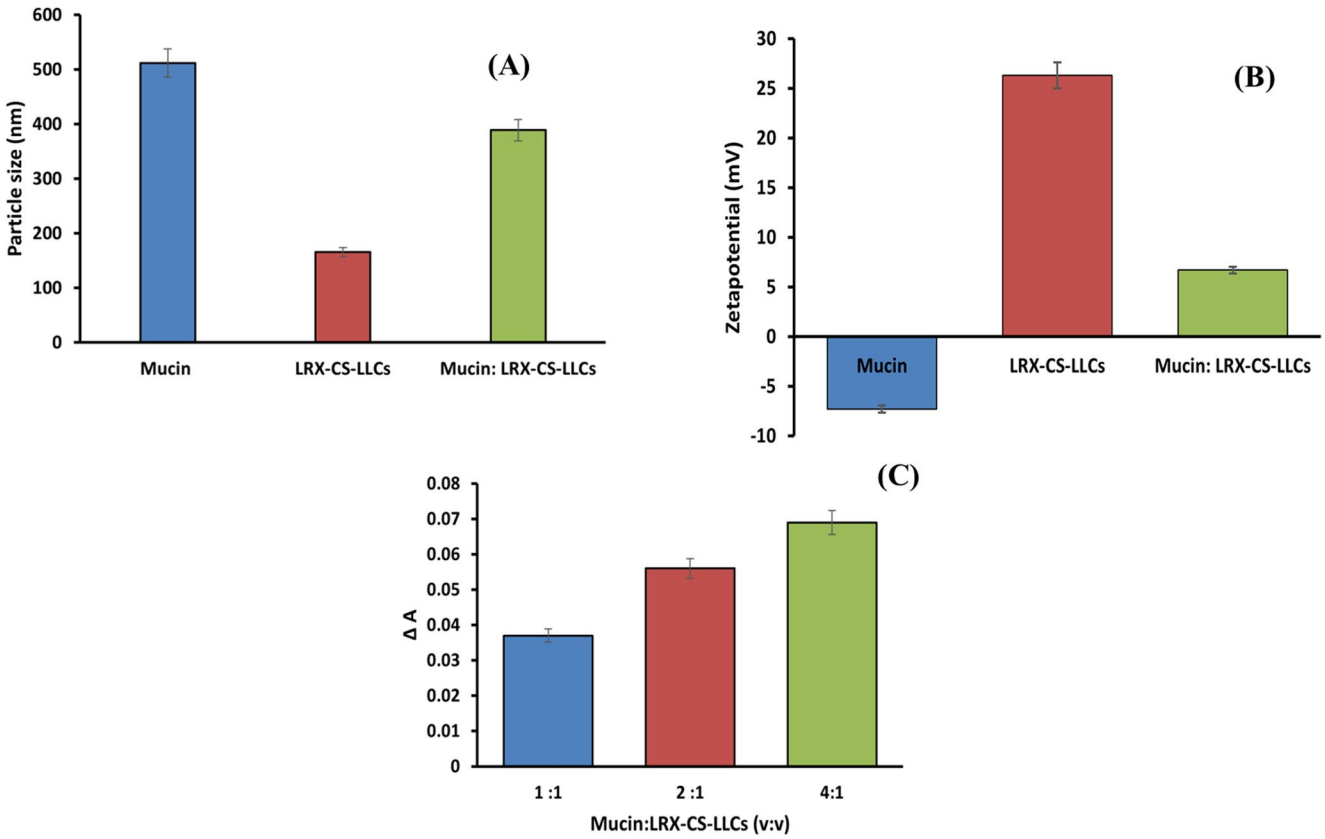



**Fig. 4** (A) Particle size and (B) zeta potential of mucin, LRX-CS-LLCs, and their mixtures. (C) Change in absorbance at various mucin: LRX-CS-LLCs volume ratios (v/v). Data are presented as mean ± SD ($n = 3$)

effects of the studied agents [96]. The present study indicates that carrageenan significantly ($p$ >0.05) elevate the the edema rate throughout the experiment, ranging from 40.38% after 1 h to 166.4% after 4 h post-injection as compared to -ve control group **(**Fig. 5**I)**. The positive control group demonstrated a substantial elevation ($p$ >0.05) in serum PGE2, COX-2, and TNF-α four hours post-injection, with values of 239.6 ± 8.2 pg/mg protein, 2.59 ± 0.04 ng/mg protein, and 159.2 ± 14.86 pg/mg protein, respectively. These values represent fold increases of 5.4, 4.47, and 3.7 compared to the negative control group **(**Fig. 5**II)**. Gross appearance and histopathological studies corroborated these findings, revealing significant edema in the left hind paw, characterized by increased redness and inflammation **(**Fig. 5**III)**. Furthermore, histopathological analysis of the positive control group revealed diffuse and focal inflammatory cell infiltrates (red arrow), scattered multinucleated giant cells (black arrow), and necrotic bone (star) **(**Fig. 6I: **B**, **C**, **D)**. LRX belongs to the oxicam class of nonsteroidal anti-inflammatory drugs, exhibiting both analgesic and antipyretic properties. This compound serves as a potent inhibitor of COX-1 and COX-2 enzymes. The analgesic action is mediated by inhibiting cyclooxygenase, reducing pain and inflammation by decreasing the synthesis of prostaglandins and thromboxanes. The action is associated with the release of endogenous dynorphin and beta-endorphin [97]. Unlike other NSAIDs, LRX does not carry a risk of specific adverse events, such as allergic reactions, due to its mechanism of inhibiting cyclooxygenase, which does not elevate leukotriene production or promote the diversion of arachidonic acid to the 5-lipoxygenase pathway. LRX exhibits a shorter elimination half-life relative to other oxicams, enhancing tolerance and suggesting its efficacy in managing pain and inflammation [98]. Furthermore, LRX demonstrated a 100-fold greater inhibitory capacity on in vitro prostaglandin production compared to tenoxicam, and it proved to be more effective than both indomethacin and piroxicam in preventing mortality induced by arachidonic acid in mice. LRX exhibited more potent anti-inflammatory effects than other NSAIDs, including piroxicam, diclofenac, ibuprofen, ketorolac, and naproxen [99, 100]. The oral administration of both pure-LRX and marketed-LRX resulted in a substantial reduction in edema rate ($p$ >0.05) throughout the experiment, demonstrating percent inhibition of 43.81% and 45.75%, respectively, after 4 h following carrageenan injection, as compared to the positive control group **(**Fig. 5**I)**. The oral administration of pure-LRX resulted in a notable reduction in PGE2 (72.35 ± 5.16 pg/mg protein), COX-2 (1.09 ± 0.09 ng/mg protein), and TNF-α (71.25 ± 2.34 pg/mg protein), demonstrating fold decreases of (3.31, 2.37, and 2.23) respectively when compared to the positive control group. Moreover, the oral administration of marketed-LRX led to a significant decrease in PGE2 (78.49 ± 5.02 pg/mg protein), COX-2 (1.24 ± 0.07 ng/mg protein), and TNF-α (83.52 ± 2.59 pg/mg protein), exhibiting fold reductions of (3.05, 2.08, and 1.9) respectively, as compared to the positive control group. No significant change was observed between the groups administered pure-Dg and marketed-Dg **(**Fig. 5**II)**. The gross examination of the left hind paws in groups administered pure and marketed medicines revealed a significant reduction in edema and erythema, indicating the anti-inflammatory efficacy of LRX in both forms **(**Fig. 5**III)**. The histopathological analysis of bone tissues revealed that the tissue sections from both the pure and marketed forms of LRX-treated groups exhibited varying degrees of treatment, with the pure group demonstrating the most favorable outcomes, akin to those seen in the normal control groups **(**Fig. 6**II**, **A)**. Conversely, the marketed group displayed a moderate infiltration of inflammatory cells **(**Fig. 6**II**, **B)**. To compare both pure-Dg and marketed-Dg with the novel formula (LRX-CS-LLCs), it was essential to include a group of rats administered the plain formula without lornoxicam (CS-LLCs). The plain CS-LLCs comprised a significant component, namely Litsea cubeba oil. Litsea cubeba, referred to as Lour. Pers. (Lauraceae), is noted for its essential oil extracted from the fruits of the plant, distinguished by a strong, fresh lemon fragrance. This oil provides numerous possible health advantages, encompassing anti-inflammatory, antibacterial, and antioxidant characteristics. The results revealed a dysregulated immune response and modified gut microbiota, indicating potential relevance for the treatment of intestinal inflammatory illnesses [41]. *Litsea cubeba* water and ethanolic extracts exhibited an inhibitory effect on adjuvant arthritis induced in rats through the down-regulation of inflammatory markers [101, 102]. The oral administration of CS-LLCs led to a significant decrease in edema rate ($p$ >0.05) during the trial, demonstrating a 44.41% ± 2.65 inhibition four hours after carrageenan injection, compared to the positive control group **(**Fig. 5**I)**. The oral delivery of CS-LLCs resulted in a notable reduction in PGE2 (85.8 ± 1.43 pg/mg protein), COX-2 (1.31 ± 0.03 ng/mg protein), and TNF-α (91.03 ± 4.45 pg/mg protein), exhibiting fold reductions of 2.79, 1.98, and 1.75, respectively, in comparison to the positive control group **(**Fig. 5**II)**. The macroscopic assessment of the left hind paws in groups treated with CS-LLCs demonstrated a notable decrease in edema and erythema, signifying the anti-inflammatory effectiveness of *Litsea cubeba* oil **(**Fig. 5**III)**. The histological examination of bone tissues indicated that the tissue sections displayed normal bone structure with a slight infiltration of inflammatory cells (red arrow) **(**Fig. 6**II**, **C)**. Ultimately, it was documented that the oral administration of LRX-CS-LLCs led to a substantial decrease in edema rate ($p$ >0.05) during the

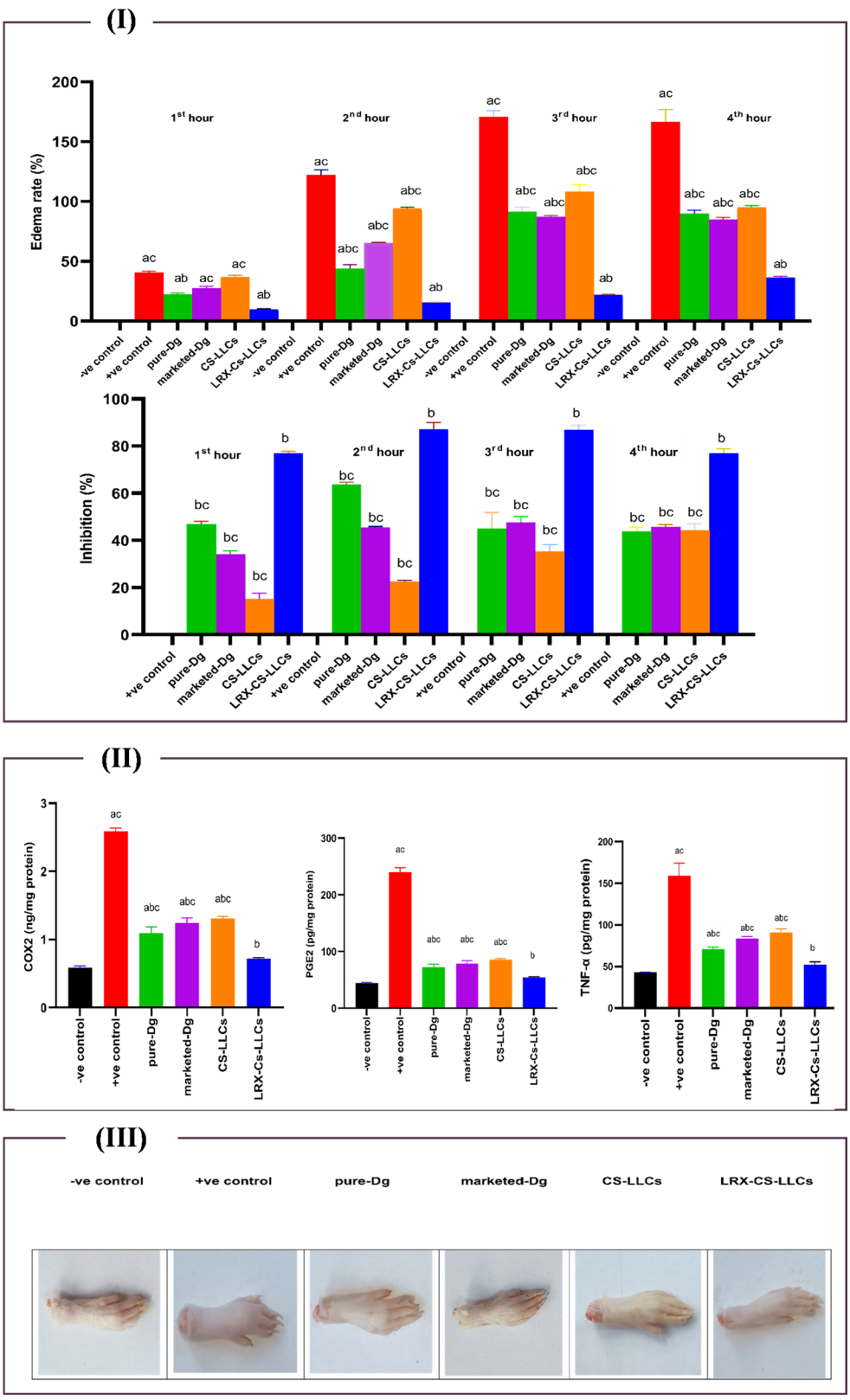
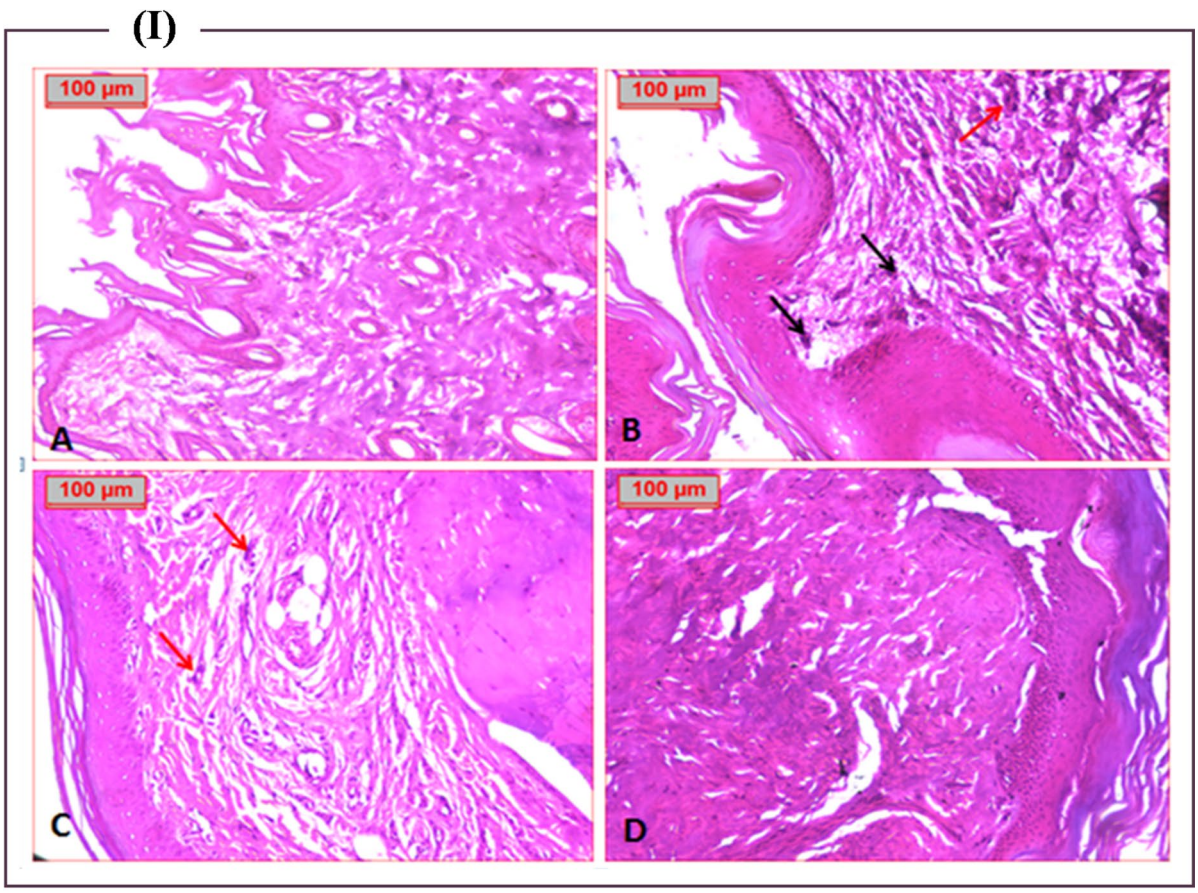



**Fig. 5** **I**: Comparative effect of pure-Dg, marketed-Dg, CS-LLCs, and LRX- CS-LLCs on carrageenan-induced inflammation in rats' hind left paws represented by edema% and inhibition% vs. control group. Edema % rate and inhibition% are defined as (mean% ± S.E) ($n=8$). $p>0.05$ is considered significant. LRX; lornoxicam, CS-LLCs; Plain Chitosan coated litsea lipid carriers, LRX- CS-LLCs; Lornoxicam loaded Chitosan coated litsea lipid carriers. **II**: Comparative effects of pure-Dg, marketed-Dg, CS-LLCs, and LRX- CS-LLCs on PGE2, COX-2, and TNF-α are represented as (mean ± S.E) ($n=8$). $p>0.05$ is considered significant. LRX; lornoxicam, CS-LLCs; CS-LLCs; Plain Chitosan coated litsea lipid carriers, LRX- CS-LLCs; Lornoxicam loaded Chitosan coated litsea lipid carriers. a represents significance from the -ve control group. b represents significance from the +ve control group. c represents significance from LRX- CS-LLCs. **III** Representative gross photographs displaying changes of the carrageenan-induced edema in the rat paw and treatment with pure-Dg, marketed-Dg, CS-LLCs, and LRX- CS-LLCs. LRX; lornoxicam, CS-LLCs; CS-LLCs; Plain Chitosan coated litsea lipid carriers, LRX- CS-LLCs; Lornoxicam loaded Chitosan coated litsea lipid carriers


(I)
100 µm
A
100 µm
B
100 µm
C
100 µm
D

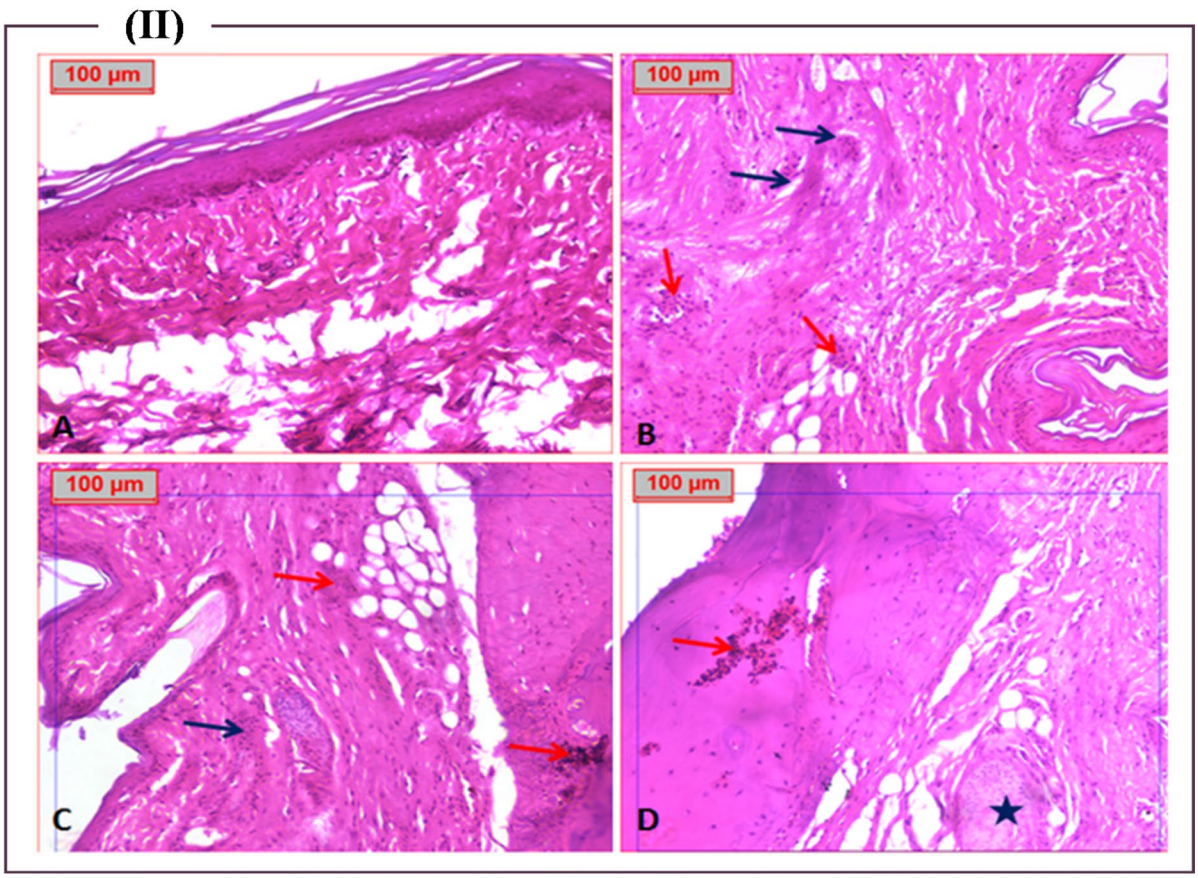

(II)
100 µm
A
100 µm
B
100 µm
C
100 µm
D

**Fig. 6** **I**: photomicrograph shows (A) -ve control group. (B, C, D)+ve control group showed bone necrosis (star), inflammatory cell infiltration (red arrow), and multinucleated giant cells (black arrow). (H&Ex200). **II**: photomicrograph shows (A) pure form treated group with normal bone structure. (B) market form with moderate inflammatory infiltrate (red arrow) and mild multinucleated giant cells (black arrow). (C) The CS-LLC group showed normal bone tissue with mild inflammatory cell infiltration (red arrow). (D) LRX- CS-LLCs group shows normal bone tissue. (H&Ex200)

trial, demonstrating a percent inhibition of 77.04% ± 1.86 four hours after carrageenan injection, in comparison to the positive control group, CS-LLCs, pure-Dg, and marketed-Dg groups Fig. 5I. The oral administration of LRX-CS-LLCs resulted in a significant reduction ($p$ >0.05) in PGE2 (54.2 ± 1.09 pg/mg protein), COX-2 (0.71 ± 0.01 ng/mg protein), and TNF-α (52.27 ± 3.43 pg/mg protein), demonstrating fold decreases of 4.42, 3.6, and 3.04, respectively, compared to the positive control group, CS-LLCs, pure-Dg, and marketed-Dg groups **(**Fig. 5**II)**. The macroscopic evaluation of the left hind paws in groups administered LRX-Cs-LLCs exhibited a normal paw morphology **(**Fig. 5**III)**. The histological examination of bone tissues indicated that the tissue sections displayed normal bone tissue **(**Fig. 6**II**, **D)**. Our results revealed that oral administration of LRX-Cs-LLCs showed an exceptional amelioration of inflammatory effect of carrageenan as compared to pure, marketed and plain group. This effect may be attributed to the addition of *Litsea cubeba* oil, which exerts inherent anti-inflammatory action; the chitosan coating, which enhances mucoadhesion, provides sustained release, and targets inflamed tissues; and the LLC formulation itself, which improves the solubility, and perdurability, of lornoxicam, ensuring efficient drug entrapment and controlled release at the site of inflammation.

## Conclusion

The LRX-CS-LLCs formulation demonstrates significant potential as an effective oral nanomedicine for managing inflammatory disorders, offering enhanced therapeutic efficacy. By exploiting the synergistic anti-inflammatory effects of *Litsea cubeba* oil, the mucoadhesive properties of chitosan, and the efficient drug-loading capacity of lipid nanocarriers, this innovative system successfully encapsulated lornoxicam, resulting in improved bioavailability and sustained release. LRX-CS-LLCs significantly alleviated inflammatory responses, as evidenced by substantial reductions in paw edema and proinflammatory cytokines. Moreover, histopathological examinations revealed preserved tissue integrity and minimal inflammatory infiltration, highlighting the formulation's protective potential. These findings establish LRX-CS-LLCs as a viable candidate for the oral treatment of inflammatory illnesses and facilitate further exploration of its applicability in a wider range of inflammation-related diseases.

**Author Contributions** All authors contributed to the study's conception and design. Material preparation, data collection, and analysis were performed by WA, AR, GA, HM, ME, RA, EM, BH, YS, SM, EY, BW, SS, and SH. The first draft of the manuscript was written by WA, AR, GA, ME, and SH and all authors commented on previous versions of the manuscript. All authors read and approved the final manuscript. Conceptualization: WA, AR, and SH. Methodology: WA, AR, GA, ME, and SH. Formal analysis and investigation: WA, AR, GA, HM, ME, RA, EM, BH, YS, SM, EY, BW, SS, and SH. Writing—original draft preparation: WA, AR, GA, ME, and SH. Writing—review and editing: WA, and AR. Funding acquisition: WA, AR, GA, ME, and SH Supervision: WA, AR, GA, and SH.

**Funding** Open access funding provided by The Science, Technology & Innovation Funding Authority (STDF) in cooperation with The Egyptian Knowledge Bank (EKB). The authors have no external funding sources to declare.

**Data Availability** No datasets were generated or analysed during the current study.

## Declarations

**Competing interests** The authors declare no competing interests.

**Open Access** This article is licensed under a Creative Commons Attribution 4.0 International License, which permits use, sharing, adaptation, distribution and reproduction in any medium or format, as long as you give appropriate credit to the original author(s) and the source, provide a link to the Creative Commons licence, and indicate if changes were made. The images or other third party material in this article are included in the article's Creative Commons licence, unless indicated otherwise in a credit line to the material. If material is not included in the article's Creative Commons licence and your intended use is not permitted by statutory regulation or exceeds the permitted use, you will need to obtain permission directly from the copyright holder. To view a copy of this licence, visit http://creativecommons.org/licenses/by/4.0/.

## References

1. Dasgupta S, Ray S, Dey S, Pal P, Mazumder B. Transdermal lipid nanocarriers: a potential delivery system for lornoxicam. Pharm Nanotechnol. 2017;5(1):32–43.
2. Said AR, Asaad GF, Shabana ME, Sayed AS, Elfeky DH, Ali HM, et al. Desosomes and desimicelles – a novel vesicular and micellar system for enhanced oral delivery of poorly soluble drug: optimization of in vitro characteristics and in vivo performance. Eur J Pharm Biopharm. 2024;200:114324.
3. Qaiser R, Pervaiz F, Noreen S, Hanan H, Shoukat H, Mahmood H, et al. Optimizing lornoxicam-loaded poly (lactic-co-glycolic acid) and (polyethylene glycol) nanoparticles for transdermal delivery: ex vivo/in vivo inflammation evaluation. Nanomedicine. 2024;19(16):1471–85.
4. Noor R, Hasan SMF, Siddiqui H, Usman FS, Naz S. Polymeric nanoparticle formulation of lornoxicam with enhanced aqueous solubility and improved anti-inflammatory effect.

5. Tung N-T, Tran C-S, Chi S-C, Dao D-S, Nguyen D-H. Integration of lornoxicam nanocrystals into hydroxypropyl methylcellulose-based sustained release matrix to form a novel biphasic release system. Int J Biol Macromol. 2022;209:441–51.
6. Shinde S, Shah R, Hosmani A, Kamble S, Sankpal P, Nalawade A et al. Formulation and Evaluation of Lornoxicam Loaded Nanosuspension Using High Pressure Homogenizer Technique.
7. Zewail MB, Asaad GF, Swellam SM, Abd-Allah SM, Hosny SK, Sallah SK, et al. Design, characterization and in vivo performance of solid lipid nanoparticles (SLNs)-loaded mucoadhesive buccal tablets for efficient delivery of lornoxicam in experimental inflammation. Int J Pharm. 2022;624:122006.
8. Habib BA, Abd El-Samiae AS, El-Houssieny BM, Tag R. Formulation, characterization, optimization, and in-vivo performance of febuxostat self-nano-emulsifying system loaded sublingual films. Drug Deliv. 2021;28(1):1321–33.
9. Khan RU, Shah SU, Rashid SA, Naseem F, Shah KU, Farid A, et al. Lornoxicam-loaded chitosan-decorated nanoemulsion: preparation and in vitro evaluation for enhanced transdermal delivery. Polymers (Basel). 2022;14(9):1922.
10. Pandey S, Shaikh F, Gupta A, Tripathi P, Yadav JS. A recent update: solid lipid nanoparticles for effective drug delivery. Adv Pharm Bull. 2021;12(1):17.
11. Zhu Y, Liang X, Lu C, Kong Y, Tang X, Zhang Y, et al. Nanostructured lipid carriers as oral delivery systems for improving oral bioavailability of nintedanib by promoting intestinal absorption. Int J Pharm. 2020;586:119569.
12. Sun B, Luo C, Li L, Wang M, Du Y, Di D, et al. Core-matched encapsulation of an oleate prodrug into nanostructured lipid carriers with high drug loading capability to facilitate the oral delivery of docetaxel. Colloids and Surfaces B: Biointerfaces. 2016;143:47–55.
13. Gao S, Tian B, Han J, Zhang J, Shi Y, Lv Q, et al. Enhanced transdermal delivery of lornoxicam by nanostructured lipid carrier gels modified with polyarginine peptide for treatment of carrageenan-induced rat paw edema. Int J Nanomedicine. 2019. https://doi.org/10.2147/IJN.S205295.
14. Palei NN, Mohanta BC, Das MK, Sabapathi ML. Lornoxicam loaded nanostructured lipid carriers for topical delivery: optimization, skin uptake and in vivo studies. J Drug Deliv Sci Technol. 2017;39:490–500.
15. Gogoi R, Loying R, Sarma N, Munda S, Pandey SK, Lal M. A comparative study on antioxidant, anti-inflammatory, genotoxicity, anti-microbial activities and chemical composition of fruit and leaf essential oils of *litsea cubeba* Pers from North-east India. Ind Crops Prod. 2018;125:131–9.
16. Liao P-C, Yang T-S, Chou J-C, Chen J, Lee S-C, Kuo Y-H, et al. Anti-inflammatory activity of Neral and geranial isolated from fruits of *Litsea cubeba* Lour. J Funct Foods. 2015;19:248–58.
17. Zewail MB, El-Gizawy SA, Asaad GF, Shabana ME, El-Dakroury WA. Chitosan coated clove oil-based nanoemulsion: an attractive option for oral delivery of Leflunomide in rheumatoid arthritis. Int J Pharm. 2023;643:123224.
18. Desai N, Rana D, Salave S, Gupta R, Patel P, Karunakaran B, et al. Chitosan: a potential biopolymer in drug delivery and biomedical applications. Pharmaceutics. 2023;15(4):1313.
19. Hongsa N, Thinbanmai T, Luesakul U, Sansanaphongpricha K, Muangsin N. A novel modified chitosan/collagen coated-gold nanoparticles for 5-fluorouracil delivery: synthesis, characterization, in vitro drug release studies, anti-inflammatory activity and in vitro cytotoxicity assay. Carbohydr Polym. 2022;277:118858.
20. Luesakul U, Puthong S, Sansanaphongpricha K, Muangsin N. Quaternized chitosan-coated nanoemulsions: a novel platform for improving the stability, anti-inflammatory, anti-cancer and transdermal properties of Plai extract. Carbohydr Polym. 2020;230:115625.
21. El-Dakroury WA, Zewail MB, Asaad GF, Abdallah HM, Shabana ME, Said AR, et al. Fexofenadine-loaded chitosan coated solid lipid nanoparticles (SLNs): a potential oral therapy for ulcerative colitis. Eur J Pharm Biopharm. 2024;196:114205.
22. Aly SH, Kandil NH, Hemdan RM, Kotb SS, Zaki SS, Abdelaziz OM, et al. GC/MS profiling of the essential oil and lipophilic extract of *Moricandia sinaica* Boiss. and evaluation of their cytotoxic and antioxidant activities. Molecules. 2023;28(5):2193.
23. Aly SH, Elissawy AM, Eldahshan OA, Elshanawany MA, Singab ANB. Variability of the chemical composition of the essential oils of flowers and the alkaloid contents of leaves of *sophora secundiflora* and *sophora tomentosa*. J Essent Oil Bear Plants. 2020;23(3):442–52.
24. Abdel-Hameed UK, Abualghaith AS, Aly SH, Soliman MM, Munshi LA, Mohammed SA, et al. GC/MS analysis and protective effects of mentha longifolia L. Essential oil against antituberculosis Drug-Induced organs toxicity in Wistar albino rats. Plants. 2024;13(22):3231.
25. Aly SH, Uba AI, Nilofar N, Majrashi TA, El Hassab MA, Eldehna WM, et al. Chemical composition and biological activity of Lemongrass volatile oil and n-hexane extract: GC/MS analysis, *in vitro* and molecular modelling studies. PLoS ONE. 2025;20(2):e0319147.
26. El-Dakroury WA, Said AR, Mageed SSA, Senbel A, Sohail SK, Rizvi SF, et al. Rivaroxaban loaded lipid carriers integrating EPA oil: a novel paradigm in drug repurposing for navigating colon targeted oral treatment for ulcerative colitis. J Drug Deliv Sci Technol. 2025. https://doi.org/10.1016/j.jddst.2025.106985.
27. Zewail MB, Nomier YA, Elesawy AE, El-Dakroury WA. Investigating the potential of quercetin-loaded chitosan-coated lipid carriers as an oral nanoplatform for depression management. Int J Biol Macromol. 2025. https://doi.org/10.1016/j.ijbiomac.2025.145569.
28. Zewail MB, Asaad GF, Shabana ME, Elbokhomy AS, Elbadry AM, Riad PY, et al. PEGylated lipid polymeric nanoparticles for management of rheumatoid arthritis. J Drug Deliv Sci Technol. 2024;101:106242.
29. Sallam A-AM, Darwish SF, El-Dakroury WA, Radwan E. Olmesartan niosomes ameliorates the Indomethacin-induced gastric ulcer in rats: insights on MAPK and Nrf2/HO-1 signaling pathway. Pharm Res. 2021;38(11):1821–38.
30. Said AR, Arafa MF, El-Dakroury WA, Alshehri S, El Maghraby GM. Bilosomes and niosomes for enhanced intestinal absorption and in vivo efficacy of cytarabine in treatment of acute myeloid leukemia. Pharmaceuticals. 2024;17(12):1572.
31. Eldeeb AM, Abdelkader DH, El Maghraby GM. Controlled antisolvent precipitation for enhanced dissolution rate and antiplatelet activity of Ticagrelor. Pharm Dev Technol. 2025;30(4):463–73.
32. Awad HA, Fetouh MI, Sultan AA, El Maghraby GM. Combined eutexia and amorphization for simultaneous enhancement of dissolution rate of triamterene and hydrochlorothiazide: preparation of orodispersible tablets. Drug Dev Ind Pharm. 2024;50(4):306–19.
33. Elkholy NE, Sultan AA, Abu-Risha SE, El Maghraby GM. Chitosan coated lipid carriers as nanoplatform for repurposed anti-breast cancer activity of niclosamide. J Drug Deliv Sci Technol. 2024;93:105414.
34. Abdelhameed MF, Asaad GF, Ragab TI, Ahmed RF, El Gendy AE-NG, Abd El-Rahman SS, et al. Oral and topical anti-inflammatory and antipyretic potentialities of araucaria bidiwillii shoot essential oil and its nanoemulsion in relation to chemical composition. Molecules. 2021;26(19):5833.
35. Buritova J, Besson J. Potent anti-inflammatory/analgesic effects of lornoxicam in comparison to other NSAIDs: a c-fos study in the rat. Inflammopharmacology. 1997;5(4):331–41.

36. Abdel-Aziz SA, Taher ES, Lan P, Asaad GF, Gomaa HAM, El-Koussi NA, et al. Design, synthesis, and biological evaluation of new pyrimidine-5-carbonitrile derivatives bearing 1,3-thiazole moiety as novel anti-inflammatory EGFR inhibitors with cardiac safety profile. Bioorg Chem. 2021;111:104890. https://doi.org/10.1016/j.bioorg.2021.104890.
37. Dawood DH, Nossier ES, Abdelhameed MF, Asaad GF, Abd El-Rahman SS. Design, synthesis, anti-inflammatory evaluation and molecular docking of novel thiophen-2-ylmethylene-based derivatives as potential TNF-α production inhibitors. Bioorg Chem. 2022;122:105726. https://doi.org/10.1016/j.bioorg.2022.105726.
38. Drury R, Wallington E. Carleton's histological technique. 5th ed. New York: Churchill Livingstone; 1980.
39. Wang H, Liu Y. Chemical composition and antibacterial activity of essential oils from different parts of *litsea cubeba*. Chem Biodivers. 2010;7(1):229–35.
40. Si L, Chen Y, Han X, Zhan Z, Tian S, Cui Q, et al. Chemical composition of essential oils of *Litsea cubeba* harvested from its distribution areas in China. Molecules. 2012;17(6):7057–66.
41. Xia L, Li R, Tao T, Zhong R, Du H, Liao Z, et al. Therapeutic potential of *litsea cubeba* essential oil in modulating inflammation and the gut microbiome. Front Microbiol. 2023;14:1233934.
42. Witayaudom P, Klinkesorn U. Effect of surfactant concentration and solidification temperature on the characteristics and stability of nanostructured lipid carrier (NLC) prepared from Rambutan (*Nephelium lappaceum* L.) kernel fat. J Colloid Interface Sci. 2017;505:1082–92.
43. Izza Nm, Suga K, Okamoto Y, Watanabe N, Bui TT, Wibisono Y, et al. Systematic characterization of nanostructured lipid carriers from cetyl palmitate/caprylic triglyceride/tween 80 mixtures in an aqueous environment. Langmuir. 2021;37(14):4284–93.
44. Vitorino C, Carvalho FA, Almeida AJ, Sousa JJ, Pais AA. The size of solid lipid nanoparticles: an interpretation from experimental design. Colloids and Surfaces B: Biointerfaces. 2011;84(1):117–30.
45. Das S, Ng WK, Tan RB. Are nanostructured lipid carriers (NLCs) better than solid lipid nanoparticles (SLNs): development, characterizations and comparative evaluations of clotrimazole-loaded SLNs and nlcs? Eur J Pharm Sci. 2012;47(1):139–51.
46. Zirak MB, Pezeshki A. Effect of surfactant concentration on the particle size, stability and potential zeta of beta carotene nano lipid carrier. Int J Curr Microbiol Appl Sci. 2015;4(9):924–32.
47. Gonzalez-Mira E, Egea M, Souto E, Calpena A, García M. Optimizing flurbiprofen-loaded NLC by central composite factorial design for oculardelivery. Nanotechnology. 2010;22(4):045101.
48. Gonzalez-Mira E, Egea M, Garcia M, Souto E. Design and ocular tolerance of flurbiprofen loaded ultrasound-engineered NLC. Colloids and Surfaces B: Biointerfaces. 2010;81(2):412–21.
49. Pogorzelski S, Watrobska-Swietlikowska D, Sznitowska M. Surface tensometry studies on formulations of surfactants with preservatives as a tool for antimicrobial drug protection characterization. J Biophys Chem. 2012. https://doi.org/10.4236/jbpc.2012.34040.
50. Hendradi E, Rosita N, Rahmadhanniar E. Effect of lipid ratio of stearic acid and oleic acid on characteristics of nanostructure lipid carrier (NLC) system of diethylammonium diclofenac. Indones J Pharm. 2017;28(4):198–204.
51. Apostolou M, Assi S, Fatokun AA, Khan I. The effects of solid and liquid lipids on the physicochemical properties of nanostructured lipid carriers. J Pharm Sci. 2021;110(8):2859–72.
52. Kanwar R, Gradzielski M, Prevost S, Kaur G, Clemens D, Appavou M-S, et al. Effect of lipid chain length on nanostructured lipid carriers: comprehensive structural evaluation by scattering techniques. J Colloid Interface Sci. 2019;534:95–104.
53. Wulff-Pérez M, Torcello-Gómez A, Gálvez-Ruíz M, Martín-Rodríguez A. Stability of emulsions for parenteral feeding: preparation and characterization of o/w nanoemulsions with natural oils and pluronic f68 as surfactant. Food Hydrocolloids. 2009;23(4):1096–102.
54. Rahmasari D, Rosita N, Soeratri W, Pharmacy. Physicochemical Characteristics, Stability, and Irritability of Nanostructured Lipid Carrier System Stabilized with Different Surfactant Ratios. Jurnal Farmasi Dan Ilmu Kefarmasian Indonesia. 2022;16. https://doi.org/10.20473/jfiki.v9i12022.8-16.
55. Khosa A, Reddi S, Saha RN. Nanostructured lipid carriers for site-specific drug delivery. Biomed Pharmacother. 2018;103:598–613.
56. Agarwal S, Kumar S, Garg R. Investigative study on impact of solid: liquid lipid ratio and stabilizer amount on some characteristics of nanostructure lipid carriers of quetiapine fumarate. Int J Pharm Investig. 2019. https://doi.org/10.5530/ijpi.2019.2.10.
57. Sangsen Y, Laochai P, Chotsathidchai P, Wiwattanapatapee R. Effect of solid lipid and liquid oil ratios on properties of nanostructured lipid carriers for oral Curcumin delivery. Adv Mater Res. 2015;1060:62–5.
58. Lasoń E, Sikora E, Ogonowski J. Influence of process parameters on properties of nanostructured lipid carriers (NLC) formulation. Acta Biochim Pol. 2013;60(4):773–7.
59. Suyuti A, Hendradi E, Purwanti T, Physicochemical, Characteristics. Entrapment Efficiency, and stability of nanostructured lipid carriers loaded coenzyme Q10 with different lipid ratios. J Res Pharm. 2023;27(3).
60. Houacine C, Adams D, Singh KK. Impact of liquid lipid on development and stability of Trimyristin nanostructured lipid carriers for oral delivery of Resveratrol. J Mol Liq. 2020;316:113734.
61. Gokce EH, Korkmaz E, Dellera E, Sandri G, Bonferoni MC, Ozer O. Resveratrol-loaded solid lipid nanoparticles versus nanostructured lipid carriers: evaluation of antioxidant potential for dermal applications. Int J Nanomed. 2012:1841–50.
62. Shah NV, Seth AK, Balaraman R, Aundhia CJ, Maheshwari RA, Parmar GR. Nanostructured lipid carriers for oral bioavailability enhancement of raloxifene: design and in vivo study. J Adv Res. 2016;7(3):423–34.
63. Kristianingsih I, Hendradi E, Siswodihardjo S, Yuwono M. Development and physicochemical characterization of nanostructured lipid carriers for entrapment of vitamin D3 prepared at different lipid ratios. Pharm Educ. 2024;24(3):204–10.
64. Duong V-A, Nguyen T-T-L, Maeng H-J. Preparation of solid lipid nanoparticles and nanostructured lipid carriers for drug delivery and the effects of preparation parameters of solvent injection method. Molecules. 2020;25(20):4781.
65. Pante GC, Castro JC, Lini RS, Romoli JCZ, Pires TY, Garcia FP, et al. Inclusion complexes of litsea Cubeba (Lour.) Pers essential oil into β-Cyclodextrin: Preparation, physicochemical Characterization, cytotoxicity and antifungal activity. Molecules. 2024;29(7):1626.
66. Xiong J, Xiong S, Guo Z, Yang M, Chen J, Fan H. Ultrasonic dispersion of nano tic powders aided by tween 80 addition. Ceram Int. 2012;38(3):1815–21.
67. Pramod K, Suneesh CV, Shanavas S, Ansari SH, Ali J. Unveiling the compatibility of Eugenol with formulation excipients by systematic drug-excipient compatibility studies. J Anal Sci Technol. 2015;6:1–14.
68. Khan Y, Durrani S, Siddique M, Mehmood M. Hydrothermal synthesis of alpha Fe2O3 nanoparticles capped by Tween-80. Mater Lett. 2011;65(14):2224–7.
69. Beraldo-de-Araújo VL, Beraldo-de-Araújo A, Costa JSR, Pelegrine ACM, Ribeiro LNM, Ed P, et al. Excipient-excipient interactions in the development of nanocarriers: an innovative statistical approach for formulation decisions. Sci Rep. 2019;9(1):10738.
70. Brito Raj S, Chandrasekhar KB, Reddy KB. Formulation, in-vitro and in-vivo pharmacokinetic evaluation of Simvastatin

nanostructured lipid carrier loaded transdermal drug delivery system. Future J Pharm Sci. 2019;5:1–14.
71. Teixeira MI, Lopes CM, Gonçalves H, Catita J, Silva AM, Rodrigues F, et al. Formulation, characterization, and cytotoxicity evaluation of lactoferrin functionalized lipid nanoparticles for riluzole delivery to the brain. Pharmaceutics. 2022;14(1):185.
72. Chen H, Zhang J, Qiao Q, Hu E, Wei Y, Pang Z, et al. A novel soluble lornoxicam-sodium chelate monohydrate with improved plasticity and tabletability. Int J Pharm. 2022;624:122060.
73. Gaglieri C, Alarcon RT, Magri R, North M, Bannach G. Development of renewable thermosetting polymers based on grape seed oil derivatives. J Appl Polym Sci. 2022;139(41):e52990.
74. Cichocki W, Kmiecik D, Baranowska HM, Staroszczyk H, Sommer A, Kowalczewski PŁ. Chemical characteristics and thermal oxidative stability of novel cold-pressed oil blends: GC, LF NMR, and DSC studies. Foods. 2023;12(14):2660.
75. Fang J-Y, Fang C-L, Liu C-H, Su Y-H. Lipid nanoparticles as vehicles for topical psoralen delivery: solid lipid nanoparticles (SLN) versus nanostructured lipid carriers (NLC). Eur J Pharm Biopharm. 2008;70(2):633–40.
76. Rodrigues da Silva GH, Paes Lemes JB, Geronimo G, de Carvalho FV, Mendonça TC, Malange KF, et al. Improved local anesthesia at inflamed tissue using the association of articaine and Copaiba oil in avocado butter nanostructured lipid carriers. Pharmaceuticals. 2023;16(4):546.
77. Chen S, Liu W, Wan J, Cheng X, Gu C, Zhou H, et al. Preparation of coenzyme Q10 nanostructured lipid carriers for epidermal targeting with high-pressure microfluidics technique. Drug Dev Ind Pharm. 2013;39(1):20–8.
78. Guilherme VA, Ribeiro LN, Alcântara AC, Castro SR, Rodrigues da Silva GH, da Silva CG, et al. Improved efficacy of naproxen-loaded NLC for temporomandibular joint administration. Sci Rep. 2019;9(1):11160.
79. Zewail M, Nafee N, Helmy MW, Boraie N. Coated nanostructured lipid carriers targeting the joints–an effective and safe approach for the oral management of rheumatoid arthritis. Int J Pharm. 2019;567:118447.
80. Pyo Y-C, Tran P, Kim D-H, Park J-S. Chitosan-coated nanostructured lipid carriers of Fenofibrate with enhanced oral bioavailability and efficacy. Colloids and Surfaces B: Biointerfaces. 2020;196:111331.
81. Gadade D, Kulkarni D, Rathi P, Pekamwar S, Joshi S. Solubility enhancement of lornoxicam by crystal engineering. Indian J Pharm Sci. 2017;79(2):277–86.
82. Popat A, Liu J, Lu GQM, Qiao SZ. A pH-responsive drug delivery system based on chitosan coated mesoporous silica nanoparticles. J Mater Chem. 2012;22(22):11173–8.
83. Bang S, Hwang I, Yu Y, Kwon H, Kim D, Park H. Influence of chitosan coating on the liposomal surface on physicochemical properties and the release profile of nanocarrier systems. J Microencapsul. 2011;28(7):595–604.
84. Yan L, Crayton SH, Thawani JP, Amirshaghaghi A, Tsourkas A, Cheng Z. A pH-responsive drug-delivery platform based on glycol chitosan–coated liposomes. Small. 2015;11(37):4870.
85. Dawoud M. Chitosan coated solid lipid nanoparticles as promising carriers for docetaxel. J Drug Deliv Sci Technol. 2021;62:102409.
86. Herdiana Y, Wathoni N, Shamsuddin S, Muchtaridi M. Drug release study of the chitosan-based nanoparticles. Heliyon. 2022. https://doi.org/10.1016/j.heliyon.2021.e08674.
87. Lang X, Wang T, Sun M, Chen X, Liu Y. Advances and applications of chitosan-based nanomaterials as oral delivery carriers: a review. Int J Biol Macromol. 2020;154:433–45.
88. Kariminia S, Shamsipur A, Shamsipur M. Analytical characteristics and application of novel chitosan coated magnetic nanoparticles as an efficient drug delivery system for ciprofloxacin. Enhanced drug release kinetics by low-frequency ultrasounds. J Pharm Biomed Anal. 2016;129:450–7.
89. Zewail MB, El-Gizawy SA, Asaad GF, El-Dakroury WA. Development of famotidine-loaded lecithin-chitosan nanoparticles for prolonged and efficient anti-gastric ulcer activity. J Drug Deliv Sci Technol. 2024;91:105196.
90. Annamalai P, Thangam EB. *Vitex trifolia* L. modulates inflammatory mediators via down-regulation of the NF-κB signaling pathway in carrageenan-induced acute inflammation in experimental rats. J Ethnopharmacol. 2022;298:115583.
91. Xiang L, Huang Q, Chen T, He Q, Yao H, Gao Y. Ethanol extract of *Paridis* rhizoma attenuates carrageenan-induced paw swelling in rats by inhibiting the production of inflammatory factors. BMC Complement Med Ther. 2023;23(1):437.
92. Takeuchi O, Akira S. Pattern recognition receptors and inflammation. Cell. 2010;140(6):805–20.
93. Szandruk-Bender M, Merwid-Ląd A, Wiatrak B, Danielewski M, Dzimira S, Szkudlarek D, et al. Novel 1, 3, 4-oxadiazole derivatives of Pyrrolo [3, 4-d] Pyridazinone exert anti-inflammatory activity without acute gastrotoxicity in the carrageenan-induced rat paw edema test. J Inflamm Res. 2021. https://doi.org/10.2147/JIR.S330614.
94. Medzhitov R. Origin and physiological roles of inflammation. Nature. 2008;454(7203):428–35.
95. Hussein SZ, Mohd Yusoff K, Makpol S, Mohd Yusof YA. Gelam honey inhibits the production of proinflammatory, mediators NO, PGE2, TNF-α, and IL-6 in carrageenan-induced acute paw edema in rats. Evidence-Based Complement Altern Med. 2012;2012(1):109636.
96. Mehrzadi S, Khalili H, Fatemi I, Malayeri A, Siahpoosh A, Goudarzi M. Zingerone mitigates carrageenan-induced inflammation through antioxidant and anti-inflammatory activities. Inflammation. 2021;44:186–93.
97. Ahmed MO, Al-Badr AA, Lornoxicam. Profiles of drug substances, excipients and related methodology. Elsevier; 2011. pp. 205–39.
98. Parada L, Marstein JP, Danilov A. Tolerability of the COX-1/COX-2 inhibitor lornoxicam in the treatment of acute and rheumatic pain. Pain Manag. 2016;6(5):445–54.
99. Buritova J, Besson J. Potent anti-inflammatory/analgesic effects of lornoxicam in comparison to other NSAIDs: a c-fos study in the rat. Inflammopharmacology. 1997;5:331–41.
100. Hussen J, Kandeel M, Shawaf T, Al-Mubarak AI, Al-Humam NA, Almathen F. Immunomodulatory effects of the cyclooxygenase inhibitor lornoxicam on phenotype and function of camel blood leukocytes. Animals. 2021;11(7):2023.
101. Lin B, Zhang H, Zhao X-X, Rahman K, Wang Y, Ma X-Q, et al. Inhibitory effects of the root extract of *litsea cubeba* (lour.) pers. on adjuvant arthritis in rats. J Ethnopharmacol. 2013;147(2):327–34.
102. Abdel-Rahman RF, El-Desoky A, Handoussa H, Meselhy MR, Asaad GF, El-Mekkawy S. LC-MS-based chemical profiling and in-vivo evaluation of the anti-inflammatory and anti-nociceptive activities of the defatted methanolic extract of Crataegus Sinaica (Rosaceae) fruits. Egypt J Chem. 2022;65(4):161–73.

**Publisher's Note** Springer Nature remains neutral with regard to jurisdictional claims in published maps and institutional affiliations.